

Atomistic Modelling of Thermal-Cycling Rejuvenation in Metallic Glasses

Baoshuang Shang^{1,2}, Weihua Wang^{3,2}, Alan Lindsay Greer⁴, and Pengfei Guan^{1,*}

¹*Beijing Computational Science Research Center, Beijing 100193, China*

²*Songshan Lake Materials Laboratory, Dongguan 523808, China*

³*Institute of Physics, Chinese Academy of Sciences, Beijing 100190, China*

⁴*Department of Materials Science and Metallurgy, University of Cambridge,
27 Charles Babbage Road, Cambridge CB3 0FS, UK.*

Cycling of a metallic glass between ambient and cryogenic temperatures can induce higher-energy states characteristic of glass formation on faster cooling. This rejuvenation, unexpected because it occurs at small macroscopic strains and well below the temperatures of thermally induced structural change, is important, for example, in improving plasticity. Molecular-dynamics simulations elucidate the mechanisms by which thermal cycling can induce relaxation (reaching lower energy) as well as rejuvenation. Thermal cycling, over tens of cycles, drives local atomic rearrangements progressively erasing the initial glass structure. This arises mainly from the heating stage in each thermal cycle, linked to the intrinsic structural heterogeneity in metallic glasses. Although, in particular, the timescales in MD simulations are shorter than in physical experiments, the present simulations reproduce many physically observed effects, suggesting that they may be useful in optimizing thermal cycling for tuning the properties of metallic glasses and glasses in general.

*pguan@csrc.ac.cn

For any type of glass of given composition, its properties can vary widely, depending on the structure reached by varying the production process and subsequent treatments¹. For metallic glasses (MGs), annealing-induced relaxation (ageing) can lead to severe embrittlement, and there is therefore a focus on the reverse process of rejuvenation. Rejuvenation can be induced by mechanical deformation²⁻⁶, by reheating and rapid quenching⁷, or irradiation⁸, but among such methods, cryogenic thermal cycling (CTC)⁹ is particularly straightforward to apply. Since the original report⁹, there have been many experimental studies of CTC applied to MGs. These have shown effects on the enthalpy¹⁰⁻²⁵, on density^{11-17, 21, 26}, on mechanical properties^{10-22, 24-31} and on structure^{19, 20, 24-27, 30, 32-34}. The most dramatic beneficial effects of rejuvenation are on the fracture behaviour: fracture toughness and impact toughness roughly doubled^{18, 28}, and toughness (critical strain-energy release rate) increased by more than a factor of five¹⁸. The underlying atomistic mechanisms of the effects of CTC clearly merit investigation.

In MGs, the atomic nearest-neighbour coordination shells are diverse, and it is increasingly recognized that there is significant structural and dynamic heterogeneity over a range of length-scales. Accordingly, the strains associated with thermal expansion/contraction must have a significant non-affine component^{35, 36} that must be associated with the development of internal stresses. While CTC was initially aimed at rejuvenation of MGs, other work^{27, 37} has shown that this treatment can also induce relaxation and oscillatory (rejuvenation-relaxation) behaviour. Relatively easy rearrangement, associated with non-directional metallic bonding, may make the effects of thermal cycling (TC) particularly significant in MGs, but the non-affine nature of thermal strains applies across all classes of non-crystalline material, and is relevant (though scarcely studied so far) for the interpretation of the evolution of their structure and properties whenever temperature changes are involved.

For MGs, molecular dynamics (MD) simulations have been useful in understanding the links between structure and dynamics, and specifically the role of structural heterogeneity³⁸. MD simulations have been used to study the effects of TC on a model Lennard-Jones (L-J) glass³⁹⁻⁴¹; in this series of studies, the temperature variation with time had a triangular waveform, i.e. there was no hold-time at the upper and lower temperatures. The TC had an amplitude as high as 2-92% of the glass-transition temperature T_g . Predominantly, the effect of TC was to lower the potential energy of the glass, and the extent of this relaxation was maximum for intermediate values of the TC amplitude. In the glass formed at the lowest cooling rate and subjected to the maximum

amplitude of TC, it was just possible to detect rejuvenation. The MD simulations showed that the extent of the stress overshoot on a tensile stress-strain curve was clearly greater for lower energy states. The simulations also allowed mapping of the distribution of clusters within which the non-affine displacements induced by TC are concentrated.

In the present work, we simulate TC of an actual glass, $\text{Cu}_{50}\text{Zr}_{50}$ (composition in at.%), and apply heating and cooling, at 10^{14} K s^{-1} , that is essentially instantaneous. We find clear rejuvenation as well as relaxation, and we map the boundary between these effects. MD simulations (generally, and in the present work) involve timescales much shorter than those typical in physical experiments. Nevertheless, we show that MD can assist in understanding the link between TC conditions and property changes. In particular, the simulations can identify the relevant length-scale of heterogeneity (a question not addressable in the original work on CTC⁹), and can identify the stage in TC mainly responsible for rejuvenation.

Results

Potential energy variation during thermal cycling. $\text{Cu}_{50}\text{Zr}_{50}$ (at.%) metallic glasses are simulated using classical MD (see Methods). Glasses formed by quenching from the liquid state at different rates Q are subjected to TC between T_a (400 K) and T_b (mostly 1 K) with hold times of t_a and t_b at these temperatures. The potential energy E is monitored, and Fig. 1a shows a case where its value (initially E_0 at the end of the quench) is higher after each cycle. The effect of the overall processing (N cycles) is characterized by the value at the end of the holding time t_a at the final temperature (400 K).

A higher Q gives an initial glass with a higher E_0 (Fig. 1b). Values of E , after up to 60 cycles, are shown for $t_a = 10 \text{ ps}$ and $t_a = 200 \text{ ps}$; for a given t_a , independent of E_0 , all the potential energies converge to a common value after about 40 cycles (Fig. 1b). Following the general interpretation of the effects of energetic processing¹, this value E_s is taken to represent a steady state in which structural damage and repair rates are in balance. Comparing $t_a = 10 \text{ ps}$ and 200 ps , the longer time allows for more relaxation and therefore gives a lower E_s . For 10 ps , all the glasses show rejuvenation on cycling; for 200 ps , the glass formed at 10^{12} K s^{-1} stays at roughly the same energy, and the most rapidly quenched glass ($Q_5 = 10^{13} \text{ K s}^{-1}$) undergoes relaxation.

For a given treatment, a more relaxed glass shows slower rejuvenation (Fig. 1b, and

Supplementary Fig. 1a where the energy changes are compared from a common starting point). This is consistent with the suggestion³⁵ that the origin of the rejuvenation is the heterogeneity of the glass structure; a more relaxed initial glass (formed on slower cooling) would have a more uniform structure. A more direct test of the effect of uniformity is obtained by MD simulations of B2 CuZr crystal. In this case, crystallographic symmetry dictates that the thermal strains are affine. The potential energy indeed shows no changes as a result of TC (see Fig. 6c and Fig. 7b later).

For a given initial glass, the effect of t_a on the E_s induced by TC is shown further in Supplementary Fig. 1b: E_s depends strongly on t_a and intersects the E_0 values of the as-quenched glasses (Fig. 2). A given as-quenched state can thus be rejuvenated or relaxed by TC (Fig. 2), just as seen in experiment²⁷. Other TC parameters being equal, there is a critical value t_c (arrowed): for $t_a < t_c$ there is rejuvenation, and for $t_a > t_c$ relaxation. The ultimate energy change on TC ($\Delta E_s = E_s - E_0$) can be mapped as a function of t_a and of the initial E_0 value of a range of glassy samples (Supplementary Fig. 2). Extrapolating the trends on the map, for a typical bulk metallic glass with cooling rate 10^4 K s^{-1} , the holding time at the upper temperature should be shorter than 100 s to achieve rejuvenation.

Upon TC, the model L-J glass cited earlier³⁹⁻⁴¹ predominantly showed relaxation. The higher of the quench rates used to form the initial glasses in the present work ($>10^{11} \text{ K s}^{-1}$) overlap the quench rates applied to the L-J system, yet our glasses formed at those higher rates still predominantly show rejuvenation upon TC (Fig. 1b). This contrasting behaviour may reflect the heating and cooling rates (Q_a and Q_b) used in our TC; these are some two orders of magnitude higher than the TC rates applied to the L-J glass, and the consequences are explored further below. In some of the TC simulations for the L-J glass, the upper temperature was as high as 92% of T_g , and this would also favour overall relaxation.

Structural and mechanical properties of cycled samples. Volume-average properties are compared for a glass with a given Q in its as-quenched state and after TC with two different t_a values to achieve steady states that represent relaxation (ageing), and rejuvenation with respect to the as-quenched glass (these three states are indicated on Supplementary Fig. 2). In each sample, the shear and bulk elastic moduli show a distribution of values. As expected, the distributions are shifted upwards in the relaxed sample and downwards in the rejuvenated sample (Fig. 3a). Atomic pair distribution functions show minor differences between the three samples. The changes

induced by rejuvenation are opposite to those induced by relaxation (Fig. 3b). The different configurations of nearest-neighbour clusters can be described as Voronoi polyhedra. For the glasses in the present work, the relative populations of the most favoured polyhedra are shown in Fig. 3c. These populations all increase on relaxation and decrease on rejuvenation. In all these respects, the relaxation and rejuvenation achieved by TC are qualitatively the same as those achieved by annealing or by forming the glass at different quench rates.

Of most practical interest is the form of the stress-strain curve for shear deformation (Fig. 3d); in a rejuvenated sample, the stress overshoot can be completely eliminated. The elimination of the overshoot is not seen for the simulated L-J glass³⁹⁻⁴¹, even when formed by quenching much faster than the maximum rate in the present work. By markedly reducing, or even eliminating, the stress overshoot at yielding, rejuvenation offers the prospect of avoiding strain localization and consequent catastrophic mechanical failure, as has been explored experimentally for rejuvenation achieved by means other than TC^{8,9}.

Vibrational behaviour during TC. MD simulations are of particular interest to characterize local structures and properties in MGs; studies show that there are low-frequency (soft) modes associated with a distribution of soft spots in the glass^{42,43}. As described in Methods, we focus on the vibrational (phonon) density of states (VDOS) $g(E)$ and the atomic participation ratio P_i in low-frequency (soft) modes (Supplementary Fig. 3).

A glass subjected to TC shows an increase in $\Delta E = E_N - E_0$, accelerating as the heterogeneity increases, before levelling off at steady state (inset, Fig. 4a). The VDOS (Fig. 4a) shows the boson peak characteristic of glasses. This peak shifts to lower energy and is more intense as the number of cycles N increases. These effects are similar to those found for heavy plastic deformation of an MG in an experimental and MD simulation study⁴⁴, in which they were associated with rejuvenated regions at shear bands.

The atomic participation ratio P_i is a suitable basis for considering temporal and spatial correlations in the MG. The Pearson correlation coefficient $p_{0,N}$ of P_i , between the initial state and after N cycles at any given location shows a clear decay towards zero as N increases (Fig. 4b). The memory of the initial state is progressively lost as the sample reaches the steady state, implying that TC can induce comprehensive structural change (α relaxation) even though the temperature is always far below T_g . As the population density of soft spots (and the boson peak intensity)

increase with the number of cycles, more rearrangement events are triggered during TC; thus the sample structure changes more and more rapidly. The decrease in correlation of P_i between two adjacent cycles as TC progresses (inset, Fig. 4b) reveals the accelerating increase in the heterogeneity of the MG.

The spatial distributions of P_i for the initial glass ($Q_1 = 10^9 \text{ K s}^{-1}$) and after the first cycle (Figs. 4c, d) show localized regions (in red) where high P_i values indicate soft spots. There are examples of both disappearance and generation of soft spots, but overall there is an increase in their population (Supplementary Fig. 4). With increasing number of cycles, the increased population appears to reach saturation, or perhaps even to decrease slightly.

The influence of TC parameters. The parameters describing the temperature profile imposed during TC are shown in Supplementary Fig. 5. Rejuvenation and relaxation are competing processes. Greater overall rejuvenation is therefore achieved if relaxation is restrained. At the upper temperature T_a of TC, structural relaxation of the MG is important in interpreting the results: shortening the holding time t_a at T_a is effective in reducing the extent of relaxation and in realizing a higher E_s (Figs. 1b, 2 and Supplementary Fig. 1b).

Relaxation can also be restrained by lowering T_b , shortening t_b , and using faster cooling and heating rates. With relaxation reduced by changing these parameters, more net rejuvenation is accumulated in each cycle (Supplementary Fig. 6). Strikingly, even though the structure is already frozen at T_b , there is still some local relaxation, indicated particularly by the local kinetic energy or temperature (Fig. 5a). Restricting relaxation during the low-temperature hold, by decreasing t_b , the distribution of local temperature $T_{b,loc}$ is more spatially heterogeneous (Figs. 5b–d) at the beginning of the heating process; this heterogeneity could be amplified and could enhance the rejuvenation during heating. The heterogeneity of local temperature $T_{b,loc}$ does not continue to decrease as t_b is prolonged; finally the decrease saturates when the heterogeneity of $T_{b,loc}$ is consistent with the structural heterogeneity. By introducing the quasi-equilibrium process (see Methods), the infinite- t_b state can be obtained. At $t_b = \infty$, the degree of rejuvenation is independent of cooling rate Q_b and lower temperature T_b , and correlated only with the heating process.

In a practical implementation of TC, there are likely to be hold times (t_a and t_b) at the upper and lower temperatures. We have shown that structural relaxation during these hold times is critical in

understanding the overall effect of TC. The effects of such relaxation cannot, of course, be studied if the TC is simulated only with a triangular-wave thermal history as in Refs. [39–41].

The causes of rejuvenation in TC. Fixing the conditions (and therefore the likely degree of relaxation) during the upper- and lower-temperature holds, we focus on the effects of the rates of cooling and heating, Q_b and Q_a . The potential-energy evolutions in one cycle with slow cooling and heating (10^{10} K s⁻¹), and with ultra-fast cooling and heating (10^{14} K s⁻¹), are shown in Fig. 6a. For low Q_b and Q_a , the potential-energy evolution is almost completely symmetrical on cooling and heating, and the value of E changes only when the temperature is changing. However, for high Q_b and Q_a , the symmetry is broken: compared to the E profile at low rate there is little change on cooling, but major changes on heating. At the start of heating at high Q_a , there is a lag before E starts to rise rapidly, overshoots its initial value E_0 , passes through a maximum, and ends the cycle higher than E_0 . We note that, if the simulation were continued to longer time, E might well decay back to E_0 ; in other words, this rejuvenation may be transient.

The evolution of E at high Q_a implies that the reheating stage plays the key role in TC-induced structural change. It is of interest to examine the correlation between the changes of potential energy $\Delta E_p = E - E_0$ and kinetic energy $\Delta E_k = E_k - E_{k,T_b}$. The increase in potential energy of the glass clearly lags behind the increase in kinetic energy during ultra-fast heating (Fig. 6b, red data points) while there is no similar effect on slow heating (Fig. 6b, blue data points). This suggests that, at least in these MD simulations, the glassy system during ultra-fast heating falls out of “equilibrium” by violating the equipartition theorem (ET); there must be local decoupling of the potential and kinetic energies. In the simulation, the degree of adherence to the ET can be adjusted by choosing different thermostats, and thereby different degrees of rejuvenation are achieved (Supplementary Fig. 7 and the associated discussion in Supplementary Material). By using the Langevin thermostat to force adherence to the ET, rejuvenation of the glass is suppressed (Fig. 6b, orange data points). Using the usual Nosé-Hoover thermostat, and applying TC to the B2 CuZr crystal there is again no rejuvenation (Fig. 6b, green data points). The contrasting effects of TC (rejuvenation or not) are shown in Fig. 6c. Thus, even at high Q_a , rejuvenation is achieved only when: (i) there is violation of the ET under the Nosé-Hoover thermostat; and (ii) there is structural heterogeneity, as in the glass but not the crystal. This is direct evidence that an external cause, the violation of the ET during ultra-fast heating, takes on its role through an internal cause, the

intrinsic structural heterogeneity, in achieving the rejuvenation in MGs.

This point can be explored further through the atomic rearrangements induced by ultra-fast heating. The local intensity of these rearrangements in a voxel i at temperature T_i is characterized by the activated rate, defined as $R_i \equiv -\Delta F_i/k_B T_i$ (see Methods), where ΔF_i is the activation energy barrier of the voxel (proportional to the local instantaneous shear modulus⁴⁵), and k_B is the Boltzmann constant. The barrier ΔF_i is directly determined by the local structural packing, which in a MG is distributed inhomogeneously. The T_i is controlled by the fast out-of-equilibrium heating. Spatial distributions of R_i at the start of the hold at T_a after ultra-fast heating are shown for different cases in Fig. 7. For the B2 CuZr crystal, R_i is controlled by the periodic structure (Fig. 7b, corresponding to the green data points in Fig. 6b), even though there can still be considerable local temperature heterogeneity generated by the NH thermostat. For the glassy state, the R_i is still homogeneous without local temperature heterogeneity, when the Langevin thermostat is used (Fig. 7c, corresponding to the orange data points in Fig. 6b). Thus, consistent with what has already been noted, the intense R_i that leads to rejuvenation upon reheating seems to require both structural and kinetic heterogeneity (Fig. 7d).

The rejuvenated glass (i.e. after TC using the NH thermostat) has the broadest distribution of R_i and the highest frequency of local atomic rearrangements during the hold at T_a (Fig. 8a). We calculated the local non-affinity \bar{D}_i to characterize the evolution of local atomic rearrangements with holding time t_a . The relatively strong correlation between the local non-affinity and the local activated rate for all atoms (Fig. 8b) in the rejuvenated case emphasizes that the atomic response is mainly controlled by the local coupling between atomic structure and temperature, which is not found in the crystal state or in the glassy state with the Langevin thermostat. The spatial evolution of the non-affinity (Fig. 9) shows that, even after a long hold at T_a , the atomic rearrangements are still correlated with the local activated rate at the start of the upper-temperature hold (circled region in Fig. 7a). Over a long enough time, however, thermal relaxation must erase such rejuvenation effects, and ultimately lead to ageing.

Discussion

Thermal cycling is known to change the properties of polycrystals of metals that have low crystallographic symmetry and therefore an anisotropic single-crystal thermal expansion coefficient^{46, 47}. For such polycrystals, the relevant microstructural length-scale is clearly the grain

diameter. It is now accepted that, well below the temperatures at which relaxation annealing would be conducted, thermal cycling, specifically CTC, is a possible method of changing the structure and properties of MGs.

From the earliest study of the effects of CTC on MGs^{9, 35}, it has been supposed that heterogeneity in the glass must play a role, but, in contrast to the polycrystalline case, the relevant length-scale has not been clear. While there are now many measurements of CTC-induced property changes in MGs, these do not give any indication of the length-scale of the relevant heterogeneity. The MD simulations in the present work do permit heterogeneity to be visualized in the spatial distributions of the local values of: the atomic participation ratio P_i (Fig. 4c,d and Supplementary Fig. 4), the temperature $T_{b,i}$ (Fig. 5b–d), the activated rate R_i (Fig. 7d), and the non-affinity D_i (Fig. 9a–d). As already noted, these various parameters are strongly correlated. Thus, as seen in these figures, they share a common length-scale: this is found to be 0.5–2.0 nm. We suggest that this length-scale is relevant for understanding TC effects in MGs.

In the TC simulations for the L-J glass, the distributions of atoms showing large non-affine displacements were mapped^{39, 41}. In early cycles of the L-J glass formed by quenching at the highest rate, large non-affine displacements were dispersed throughout the sample, but in all other cases, the atoms showing such displacements were dispersed as small clusters. The distribution and size of these clusters are similar to, for example, those of the local participation ratio P_i (Fig. 4c,d).

This length-scale is below the resolution limit of common imaging techniques. For electron microscopy, for example, we note that the thickness of the electron-transparent thin foil is 1 to 2 orders of magnitude greater than the heterogeneity size – accordingly, the detection of structural heterogeneity is hindered by projection effects. Nanoprobe studies of MG surfaces do suggest heterogeneity on the scale down to about 1.5 nm [48], broadly consistent with the present work. Length-scales of tens of nm⁴⁹, or even tens of μm ¹⁸, have also been suggested to describe the heterogeneity in MGs, but such scales cannot be studied with the simulation methods in the present work. If the length-scale of the heterogeneity giving TC effects is 0.5–2.0 nm, that is favourable for the potential application of TC to treat MG components in MEMS and NEMS devices.

An experimental study of a $\text{Cu}_{46}\text{Zr}_{46}\text{Al}_7\text{Gd}_1$ BMG⁵⁰ found that TC has a strong rejuvenation effect on some properties (notably the initial yield load in nanoindentation, F_y) and only a weak effect on others (e.g. hardness, H). The relaxation effect of annealing can be reversed by TC for F_y ,

but not for H . These effects could be consistently interpreted by considering the MG to contain soft spots in a relatively rigid matrix: TC affects mainly the soft spots, increasing both their population density and the ease of shear within them. It was inferred that a property such as F_y is strongly affected by the distribution of soft spots, while H depends mainly on the rigid matrix, which is barely affected by TC. The soft spots were associated with shear-transformation zones, and therefore directly connected with improved plasticity⁵⁰.

The present work is remarkably consistent with this picture. As noted above, the simulations give spatial distributions of P_i , R_i and D_i that all show soft spots. It is clear that TC does specifically affect the nature and population of those soft spots. Furthermore, TC is shown (Fig. 3d) to affect the onset of plastic flow much more than its continuation, consistent with the different effects measured⁵⁰ for F_y and H .

It is evident both from physical measurements^{27, 37} and from the simulations in the present work (Fig. 2, Supplementary Fig. 2) that the effect of TC on MGs is delicately balanced between relaxation and rejuvenation. The dynamic nature of that balance can be better understood by noting that even when, for example, there is a strong overall rejuvenation, soft spots are disappearing as well as appearing (Fig. 4c,d).

In the present work, our aim has been to advance understanding of the effects of TC on the structure and properties of MGs, and in particular how a given MG can be rejuvenated to states of higher energy or aged to lower energy. We have conducted molecular-dynamics (MD) atomistic simulations of cycling $\text{Cu}_{50}\text{Zr}_{50}$ (at.%) glasses between $T_a = 400$ K and $T_b = 1$ K. The simulations do allow exploration of the effects of a range of thermal-cycling parameters. Depending, for example, on the quench rate used to form the glass, and on the hold time at the upper temperature during cycling, the MG can undergo either rejuvenation or ageing as a result of TC.

Focusing on rejuvenation, the effects of TC are clear in progressively increased potential energy and reduced structural correlation with the as-cast glass, while the heterogeneity in the rejuvenated glass increases. As the heterogeneity increases, the rejuvenation (quantified as the potential energy) accelerates, until levelling off at a steady-state value. Rejuvenated glasses show reduced populations of the most common atom-centred clusters, reduced elastic moduli, and an increased boson peak. The effects in the simulations are in broad qualitative agreement with published experimental findings.

The simulations show that, during one cycle, the excitation (externally driven increase in

potential energy) occurs in large measure only on heating from the lower temperature T_b to the upper temperature T_a . We conclude that rejuvenation in TC has two causes. The first, heterogeneity in local coefficient of thermal expansion, was suggested in early work^{9, 35} and computed by some of us³⁶, but is negligible in the present MD simulations. The second, hysteresis arising from a violation of the equipartition theorem, is found at the exceptionally high heating rates in the present simulations, but itself relies on the structural heterogeneity intrinsic to the glassy state.

The simulated Cu-Zr glasses show conclusively that cryogenic thermal cycling is capable of inducing local atomic displacements that, over progressive cycles, destroy all memory of the as-quenched structure of the glass. The properties of the TC-treated glass reach a steady state that may be relaxed or rejuvenated with respect to the as-quenched state, depending on the energy of the initial glass and the TC conditions. Simulations of the kind demonstrated in the present work, will allow exploration of the effects of TC parameters and thereby help in optimizing TC treatments.

Methods

Simulation procedures and samples. Molecular-dynamics (MD) simulations were performed with the LAMMPS package⁵¹ for Cu₅₀Zr₅₀ (at.%) metallic glass with realistic embedded-atomic-method potentials⁵². The MD time step was set to 2 fs, and a constant pressure and temperature (NPT) ensemble was employed in which the temperature and pressure were controlled by the Nosé-Hoover^{53, 54} and Parrinello-Rahman⁵⁵ methods respectively. To check the thermal-expansion effect in MD, we also used a constant volume and temperature (NVT) ensemble (Supplementary Fig. 8); this gave similar results. For temperature control in the heating step in TC, we also used the Berendsen thermostat (B)⁵⁶, the rescaled atomic velocity approach (R), and Langevin thermostat (L)⁵⁷. The model system contained 10,000 atoms in a cubic box with periodic boundary conditions; we compared results with a larger system, but found no size effect. We first kept the system at 2500 K (far above the melting point) for 10 ns, and then the melt was quenched at selected rates from 2500 K to T_a to prepare the initial glassy samples with different thermal histories.

Thermal cycling (TC). The different rates of quenching, $Q_i = 10^9, 10^{10}, 10^{11}, 10^{12}$ or 10^{13} K s⁻¹, give virtual glassy samples in different initial states. We set the upper temperature $T_a = 400$ K, which is 54% of the glass-transition temperature T_g for this model system, and therefore below the temperatures normally associated with α and β thermal relaxations. Subsequent thermal cycling (Fig. 1a) consisted of cooling to the lower temperature T_b (set at 1 K), holding at T_b , and heating back to T_a , at which all properties are measured. The cooling and heating were near-instantaneous, at $\sim 10^{14}$ K s⁻¹ (chosen to be faster than the quenching rates used to form the glasses). The hold times at the lower and upper temperatures are t_b , set at 100 ps, and t_a , treated as variable to examine possible relaxation effects. The potential energy after each cycle is monitored as a function of the number of cycles N and of t_a . TC induces changes in potential energy, $\Delta E = E_N^{t_a} - E_0$, where E_0 is the value for the as-quenched sample: $\Delta E > 0$ represents rejuvenation (Fig. 1a) and $\Delta E < 0$ represents relaxation (ageing). A schematic of simulation parameters in one cycle is shown in Supplementary Fig. 5.

Mechanical properties. To measure mechanical properties, simple shear deformation with shear rate 10^7 s⁻¹ was employed to obtain the strain-stress curves (Fig. 3d) of each type of sample at 400 K. Ten independent loading runs were employed for each sample to ensure statistical validity.

Three types of samples (Supplementary Fig. 2, the three white points in the map): as-quenched (Q_5), aged ($t_a = 200$ ps), and rejuvenated ($t_a = 10$ ps) were selected to investigate the influence of TC.

Quasi-equilibrium state ($t_b = \infty$). As in a crystalline solid, in the glass at low temperature structural relaxation is suppressed. The thermal motion in the glass can then be regarded as atomic vibration around the inherent structure⁵⁸. At the low temperature in our case, $T_b = 1$ K, this atomic vibration can be approximated as a harmonic oscillator. In a classical system, the equipartition theorem⁵⁹ should work well at equilibrium, and thus for the quasi-equilibrium glassy state, we have $E_k = \Delta E_p$, where E_k is the kinetic energy of the system, and ΔE_p is the difference between the potential energy at temperature T_b and the potential energy of the inherent structure.

In the MD simulations, first we used a conjugate-gradient algorithm to obtain the inherent structure. We injected kinetic energy $E_k = 2k_B$ into that structure, and used the microcanonical ensemble (NVE) to relax the system. Accordingly, the system is in the quasi-equilibrium state when $E_k = \Delta E_p = 1k_B$. We have checked whether the sample starts from the quasi-equilibrium state in each cycle. In the simulation, the states obtained by TC are insensitive to the quench rate Q_b , holding time t_b and minimization method. For the NVE relaxation, we used 2 ps in the simulation, and longer relaxation times do not change the results.

Local property characterization. The local parameters centred in $30 \times 30 \times 30$ voxels (cubic, of side length ~ 1 nm) were calculated by a coarse-grained method.

Vibrational density of states (VDOS) and atomic participation ratio (P_i). The dynamic matrix (DM) was calculated from energy-minimized samples, and the DM was diagonalized to obtain the vibrational density of states and the vibration mode. To extract the contribution of the Debye vibration mode, we used the reduced VDOS, $VDOS/\omega^2$. The boson peak in the low-frequency regime is shown in Fig. 4a. The participation ratio (PR) was calculated following the method used in Ref. [43], using a low 1% vibration mode. The PR of atom i is given by $P_i = \sum_{\mathbf{N}(\omega \in 1\%)} \bar{\mathbf{e}}_{\omega}^i \cdot \bar{\mathbf{e}}_{\omega}^i$, where $\bar{\mathbf{e}}_{\omega}^i$ is the vector polarization at atom i at vibration frequency ω . The local PR of voxel i (\bar{P}_i) is given by $\bar{P}_i = \frac{1}{N_i} \sum_{j \in N_i} P_j$, where N_i is the number of atoms in voxel i , and P_j is the PR of atom j . In glasses, the low-frequency vibration modes are localized, and the related atomic participation ratio P_i can be regarded as an indicator of local structural instability. Thus, the evolution of P_i could provide deep understanding about the local structural responses during rejuvenation.

Local activated rate. We define the local activated rate R_i of voxel i as

$$R_i = e^{-\frac{\Delta F_i}{k_B T_i}}$$

where ΔF_i is the local energy barrier, and T_i is the local temperature, of voxel i .

In the ‘shoving model’ for molecular rearrangements in liquids⁴⁵, the relaxation energy barrier is dominated by elastic energy, and the relaxation between energy barrier and elastic energy is even true at local scale⁶⁰. Following the formula by Wang et al.⁶¹, here we assume that the formula still works at the local scale. Then the local energy barrier ΔF_i can be expressed as:

$$\Delta F_i = \frac{1}{11} (10G_\infty^i + B_\infty^i) \frac{V_i}{N_i}$$

where G_∞^i and B_∞^i are the local instantaneous shear and bulk moduli, respectively; V_i is the coarse-grained volume of, and N_i is the number of atoms contained in, voxel i . Following the method used in Ref. [62], we use the local Cauchy-Born modulus to approximate the instantaneous modulus. The local temperature T_i is defined by:

$$k_B T_i \equiv \frac{2}{3} E_k^i = \frac{1}{3N_i} \sum_{j \in N_i} m_j \vec{v}_j \cdot \vec{v}_j$$

where E_k^i is the local kinetic energy, \vec{v}_j is the velocity of atom j and m_j is the mass of atom j .

Local non-affinity. Following the work of Falk & Langer⁶³, the non-affinity of atom j can be defined as

$$D_j^2(t, \Delta t) = \frac{1}{N_j} \sum_{k \in N_j} [\vec{r}_{jk}(t + \Delta t) - \gamma_j \vec{r}_{jk}(t)]^2$$

where $\gamma_j = Y_j^{-1} \cdot X_j$, $Y_j = \sum_{k \in N_j} [\vec{r}_{jk}(t)]^T [\vec{r}_{jk}(t)]$, $X_j = \sum_{k \in N_j} [\vec{r}_{jk}(t + \Delta t)]^T [\vec{r}_{jk}(t)]$, and $\vec{r}_{jk} = \vec{r}_k - \vec{r}_j$ is the position vector of atom j at time t . We take D_j , the square root of D_j^2 , as the non-affinity of atom j , and local non-affinity of voxel i is given by

$$\bar{D}_i(t, \Delta t) = \frac{1}{N_i} \sum_{j \in N_i} D_j(t, \Delta t)$$

We take the beginning of the holding time at T_a as the reference time ($t_a = 0$), as shown by the circled region in Fig. 7a, and investigate the evolution of non-affinity with t_a .

Pearson correlation coefficient. This coefficient is employed to characterize the correlation between X and Y as

$$\rho_{X,Y} = \frac{E[XY] - E[X]E[Y]}{\sqrt{E[X^2] - E[X]^2} \sqrt{E[Y^2] - E[Y]^2}}$$

where $E[\cdot]$ is the expectation.

References

- [1] Sun, Y. H., Concustell, A. & Greer, A. L. Thermomechanical processing of metallic glasses: extending the range of the glassy state. *Nat. Rev. Mater.* **1**, 16039 (2016).
- [2] Bei, H., Xie, S. & George, E. P. Softening caused by profuse shear banding in a bulk metallic glass. *Phys. Rev. Lett.* **96**, 105503 (2006).
- [3] Song, K. K., Pauly, S., Zhang, Y., Scudino, S., Gargarella, P., Surreddi, K. B., Kühn, U. & Eckert, J. Significant tensile ductility induced by cold rolling in $\text{Cu}_{47.5}\text{Zr}_{47.5}\text{Al}_5$ bulk metallic glass. *Intermet.* **19**, 1394–1398 (2011).
- [4] Meng, F., Tsuchiya, K., Il, S. & Yokoyama, Y. Reversible transition of deformation mode by structural rejuvenation and relaxation in bulk metallic glass. *Appl. Phys. Lett.* **101**, 121914 (2012).
- [5] Ding, G., Li, C., Zaccone, A., Wang, W. H., Lei, H. C., Jiang, F., Ling, Z., & Jiang M. Q. Ultrafast extreme rejuvenation of metallic glasses by shock compression. *Sci. Adv.* **5**, eaaw6249 (2019).
- [6] Pan, J., Ivanov, Yu. P., Zhou, W. H., Li, Y. & Greer, A. L. Strain-hardening and suppression of shear-banding in rejuvenated bulk metallic glass. *Nature* **578**, 559–562 (2020).
- [7] Wakeda, M., Saida, J., Li, J. & Ogata, S. Controlled rejuvenation of amorphous metals with thermal processing. *Sci. Rep.* **5**, 10545 (2015).
- [8] Magagnosc, D. J., Ehrbar, R., Kumar, G., He, M. R., Schroers, J. & Gianola, D. S. Tunable tensile ductility in metallic glasses. *Sci. Rep.* **3**, 1096 (2013).
- [9] Ketov, S. V., Sun, Y. H., Nachum, S., Lu, Z., Checchi, A., Beraldin, A. R., Bai H. Y., Wang, W. H., Louzguine-Luzgin, D. V., Carpenter, M. A. & Greer, A. L. Rejuvenation of metallic glasses by non-affine thermal strain. *Nature* **524**, 200–203 (2015).
- [10] Song, W., Meng, X., Wu, Y., Cao, D., Wang, H., Liu, X., Wang, X. & Lu, Z. Improving plasticity of the $\text{Zr}_{46}\text{Cu}_{46}\text{Al}_8$ bulk metallic glass via thermal rejuvenation. *Science Bull.* **63**, 840–844 (2018).
- [11] Guo, W., Yamada, R. & Saida, J. Rejuvenation and plasticization of metallic glass by deep cryogenic cycling treatment. *Intermetal.* **93**, 141–147 (2018).
- [12] Guo, W., Yamada, R., Saida, J., Lü, S. & Wu, S. Various rejuvenation behaviors of Zr-based metallic glass by cryogenic cycling treatment with different casting temperatures. *Nanos. Res. Lett.* **13**, 398 (2018).
- [13] Guo, W., Saida, J., Zhao, M., Lü, S. & Wu, S. Thermal rejuvenation of an Mg-based metallic glass. *Metall. Mater. Trans. A* **50A**, 1125–1129 (2019).
- [14] Guo, W., Shao, Y., Saida, J., Zhao, M., Lü, S. & Wu, S. Rejuvenation and plasticization of

- Zr-based bulk metallic glass with various Ta content upon deep cryogenic cycling, *J. Alloy. Comp.* **795**, 314–318 (2019).
- [15] Guo, W., Saida, J., Zhao, M., Lü, S. & Wu, S. Rejuvenation of Zr-based bulk metallic glass composite upon deep cryogenic cycling. *Mater. Lett.* **247**, 135–138 (2019).
- [16] Guo, W., Saida, J., Zhao, M., Lü, S. & Wu, S. Unconspicuous rejuvenation of a Pd-based metallic glass upon deep cryogenic cycling treatment. *Mater. Sci. Eng. A* **759**, 59–64 (2019).
- [17] Guo, W., Saida, J., Zhao, M., Lü, S. & Wu, S. Non-thermal crystallization process in heterogeneous metallic glass upon deep cryogenic cycling treatment. *J. Mater. Sci.* **54**, 8778–8785 (2019).
- [18] Li, B. S., Xie, S. & Kruzic, J. J. Toughness enhancement, and heterogeneous softening of a cryogenically cycled Zr-Cu-Ni-Al-Nb bulk metallic glass. *Acta Mater.* **176**, 278–288 (2019).
- [19] Samavatian M., Gholamipour, R., Amadeh, A. A. & Mirdamadi, S. Extra rejuvenation of $Zr_{55}Cu_{30}Al_{10}Ni_5$ bulk metallic glass using elastostatic loading and cryothermal treatment interaction. *J. Non-Cryst. Solids* **506**, 39–45 (2019).
- [20] Sohrabi, S., Ri, M. C., Jiang, H. Y., Gu, L., Wen, P., Sun, Y. H. & Wang, W. H. Prominent role of chemical heterogeneity on cryogenic rejuvenation and thermomechanical properties of La–Al–Ni metallic glass. *Intermetallics* **111**, 106497 (2019).
- [21] Guo, W., Shao, Y., Zhao, M., Lü, S. & Wu, S. Varying the treating conditions to rejuvenate metallic glass by deep cryogenic cycling treatment. *J. Alloys Comp.* **819**, 152997 (2020).
- [22] Gu, J.-L., Luan, H.-W., Zhao, S.-F., Bu, H.-T., Si, J.-J., Shao, Y. & Yao, K.-F. Unique energy-storage behavior related to structural heterogeneity in high-entropy metallic glass. *Mater. Sci. Eng. A* **786**, 139417 (2020).
- [23] Zhang, W., Xiang, Q. C., Ma, C. Y., Ren, Y. L. & Qiu, K. Q. Relaxation-to-rejuvenation transition of a Ce-based metallic glass by quenching/cryogenic treatment performed at sub- T_g . *J. Alloys Comp.* **825**, 153997 (2020).
- [24] Ketkaew, J., Yamada, R., Wang, H., Kuldinow, D., Schroers, B. S., Dmowski, W., Egami, T. & Schroers, J. The effect of thermal cycling on the fracture toughness of metallic glasses. *Acta Mater.* **184**, 100–108 (2020).
- [25] Di, S., Wang, Q., Zhou, J., Shen, Y., Li, J., Zhu, M., Yin, K., Zeng, Q., Sun, L. & Shen, B. Enhancement of plasticity for FeCoBSiNb bulk metallic glass with superhigh strength through cryogenic thermal cycling. *Scripta Mater.* **187**, 13–18 (2020).
- [26] Xiao, H. B., Wang X. D., Zhang, P., Cao, X. Z., Chen, Y., Le, T., Cao, Q. P., Zhang, D. X. & Jiang, J.

- Z. Contribution of cryogenic thermal cycling to the atomic dynamics in a La-based bulk metallic glass with different initial states. *J. Appl. Phys.* **127**, 205104 (2020).
- [27] Ketov S. V., Trifonov, A. S., Ivanov, Y. P., Churyumov, A. Yu., Lubenchenko, A. V., Batrakov, A. A., Jiang, J., Louzguine-Luzgin, D. V., Eckert, J., Orava, J. & Greer, A. L. On cryothermal cycling as a method for inducing structural changes in metallic glasses. *NPG Asia Mater.* **10**, 137–145 (2018).
- [28] Grell, D., Dabrock, F. & Kerscher, E. Cyclic cryogenic pretreatments influencing the mechanical properties of a bulk glassy Zr-based alloy. *Fatigue Fract. Eng. Mater. Struct.* **41**, 1330–1343 (2018).
- [29] Krämer, L., Maier-Kiener, V., Champion, Y., Sarac, B. & Pippan, R., Activation volume and energy of bulk metallic glasses determined by nanoindentation. *Mater. Design* **155**, 116–124 (2018).
- [30] Samavatian, M., Gholamipour, R., Amadeh, A. A. & Mirdamadeh, S. Correlation between plasticity and atomic structure evolution of a rejuvenated bulk metallic glass. *Metall. Mater. Trans. A* **50A**, 4743–4749 (2019).
- [31] Zheng, H., Zhu, L., Jiang, S. S., Wang, Y. G. & Chen, F. G. Recovering the bending ductility of the stress-relieved Fe-based amorphous alloy ribbons by cryogenic thermal cycling. *J. Alloys Comp.* **790**, 529–535 (2019).
- [32] Abrosimova G., Volkov, N., Tuan, T. V., Pershina, E. & Aronin, A. Cryogenic rejuvenation of Al-based amorphous-nanocrystalline alloys. *Mater. Lett.* **240**, 150–152 (2019).
- [33] Abrosimova, G., Volkov, N., Pershina, E., Tuan, T. V. & Aronin, A. Amorphous structure rejuvenation under cryogenic treatment of Al-based amorphous-nanocrystalline alloys. *J. Non-Cryst. Solids* **28**, 119751 (2020).
- [34] Das, A., Dufresne, E. M. & Maaß, R. Structural dynamics and rejuvenation during cryogenic cycling in a Zr-based metallic glass. *Acta Mater.* **196**, 723–732 (2020).
- [35] Hufnagel, T. C. Metallic glasses: Cryogenic rejuvenation. *Nat. Mater.* **14**, 867–868 (2015).
- [36] Shang, B. S., Guan, P. F. & Barrat, J.-L. Role of thermal expansion heterogeneity in the cryogenic rejuvenation of metallic glasses. *J. Phys. Mater.* **1**, 015001 (2018).
- [37] Wang, X., Shao, Y., Gong, P. & Yao, K. F. The effect of simulated thermal cycling on thermal and mechanical stability of a Ti-based bulk metallic glass. *J. Alloys Comp.* **575**, 449–454 (2013).
- [38] Ma, E. Tuning order in disorder. *Nat. Mater.* **14**, 547–552 (2015).
- [39] Priezjev, N. V. The effect of cryogenic thermal cycling on aging, rejuvenation, and mechanical properties of metallic glasses. *J. Non-Cryst. Solids*, **503–504**, 131–138 (2019).
- [40] Liu, Q.-L. & Priezjev, N. V. The influence of complex thermal treatment on mechanical properties of

- amorphous materials. *Comput. Mater. Sci.* **161**, 93–8 (2019).
- [41] Priezjev, N. V. Potential energy states and mechanical properties of thermally cycled binary glasses. *J. Mater. Res.* **34**, 2664–2671 (2019).
- [42] Manning, M. L. & Liu, A. J. Vibrational modes identify soft spots in a sheared disordered packing. *Phys. Rev. Lett.* **107**, 108302 (2011).
- [43] Ding, J., Patinet, S., Falk, M. L., Cheng, Y. Q. & Ma, E. Soft spots and their structural signature in a metallic glass. *Proc. Nat. Acad. Sci. U.S.A.*, **111**, 14052–14056 (2014).
- [44] Bünz, J., Brink, T., Tsuchiya, K., Meng, F. Q., Wilde, G. & Albe, K. Low temperature heat capacity of a severely deformed metallic glass. *Phys. Rev. Lett.* **112**, 135501 (2014).
- [45] Dyre, J. C. Colloquium: The glass transition and elastic models of glass-forming liquids. *Rev. Mod. Phys.* **78**, 953–972 (2006).
- [46] Ma, B. M. *Nuclear Reactor Materials and Applications*, Sect. 6.7.2., 149–151 (Van Nostrand, 1983).
- [47] Yuan, C., Wang, Y., Sang, D., Li, Y., Jing, L., Fu, R. & Zhang, X. Effects of deep cryogenic treatment on the microstructure and mechanical properties of commercial pure zirconium. *J. Alloy. Comp.* **619**, 513–519 (2015).
- [48] Liu, Y. H., Wang, D., Nakajima, K., Zhang, W., Hirata, A., Nishi, T., Inoue, A. & Chen, M. W. Characterization of nanoscale mechanical heterogeneity in a metallic glass by dynamic force microscopy. *Phys. Rev. Lett.* **106**, 125504 (2011).
- [49] Wagner, H., Bedorf, D., Küchemann, S., Schwabe, M., Zhang, B., Arnold, W. & Samwer, K. Local elastic properties of a metallic glass. *Nature Mater.* **10**, 439–442 (2011).
- [50] Meylan, C. M., Papparotto, F., Nachum, S., Orava, J., Miglierini, M., Basykh, V., Ferenc, J., Kulik, T., Greer, A. L. Stimulation of shear-transformation zones in metallic glasses by cryogenic thermal cycling. *J. Non-Cryst. Solids* **548**, 120299 (2020).
- [51] Plimpton, S. Fast parallel algorithms for short-range molecular dynamics. *J. Comput. Phys.* **117**, 1–19 (1995).
- [52] Mendelev, M. I., Kramer, M. J., Ott, R. T., Sordelet, D. J., Yagodin, D. & Popel, P. Development of suitable interatomic potentials for simulation of liquid and amorphous CuZr alloys. *Philos. Mag.* **89**, 967–987 (2009).
- [53] Nosé, S. A unified formulation of the constant temperature molecular dynamics methods. *J. Chem. Phys.* **81**, 511–519 (1984).
- [54] Hoover, W. G. Canonical dynamics: Equilibrium phase-space distributions. *Phys. Rev. A* **31**, 1695–1697 (1985).

- [55] Parrinello, M. & Rahman, A. Polymorphic transitions in single crystals: A new molecular dynamics method. *J. Appl. Phys.* **52**, 7182–7190 (1981).
- [56] Berendsen H., Postma, J., van Gunsteren, W. F., DiNola, A. & Haak, J. Molecular dynamics with coupling to an external bath. *J. Chem. Phys.* **81**, 3684–3690 (1984).
- [57] Schneider, T. & Stoll, E. Molecular-dynamics study of a three-dimensional one-component model for distortive phase transitions. *Phys. Rev. B* **17**, 1302–1322 (1978).
- [58] Stillinger, F. H. & Weber, T. A. Hidden structure in liquids. *Phys. Rev. A* **25**, 978–989 (1982).
- [59] Huang, K. *Statistical Mechanics*. 2nd edn, (John Wiley & Sons, New York, NY, 1987).
- [60] Shang, B. S., Rottler, J., Guan, P. F. & Barrat, J.-L. Local versus global stretched mechanical response in a supercooled liquid near the glass transition. *Phys. Rev. Lett.* **122**, 105501 (2019).
- [61] Wang, J. Q., Wang, W. H., Liu, Y. H. & Bai, H. Y. Characterization of activation energy for flow in metallic glasses. *Phys. Rev. B* **83**, 012201 (2011).
- [62] Mizuno, H., Mossa, S. & Barrat, J.-L. Measuring spatial distribution of the local elastic modulus in glasses. *Phys. Rev. E* **87**, 042306 (2013).
- [63] Falk, M. L. & Langer, J. S. Dynamics of viscoplastic deformation in amorphous solids. *Phys. Rev. E* **57**, 7192–7205 (1998).

Acknowledgements

This work was supported by The Science Challenge Project (TZ2018004), Guangdong Major Project of Basic and Applied Basic Research, China (Grant No. 2019B030302010), the NSF of China (Grant Nos. 51571111, 51271195, 51601009, U1930402) and MOST 973 Program (2015CB856800). T.C. Wang, J.-L. Barrat are thanked for discussions. A.L.G. acknowledges support from the European Research Council under the European Union's Horizon 2020 research and innovation programme (grant ERC-2015-AdG-695487: ExtendGlass). B.S.S. and P.F.G. acknowledge the computational support from the Beijing Computational Science Research Center (CSRC).

Author contributions

P.F.G. and B.S.S. conceived and designed the work. B.S.S. and P.F.G. conducted the simulations. All the authors contributed to the analysis and interpretation of the data. B.S.S., W.H.W., A.L.G. and P.F.G. wrote the manuscript.

Competing interests: The authors declare no competing financial interests.

Figure Captions

Fig. 1 Thermal cycling (TC) and its effect on simulated $\text{Cu}_{50}\text{Zr}_{50}$ glass. **(a)** The initial glassy states are prepared by quenching at various rates Q_i , and then subjected to TC between T_a and T_b . The holding times at T_b and T_a are t_b and t_a respectively. After N thermal cycles, the potential energy has risen by ΔE relative to its value E_0 in the as-quenched glass. **(b)** The initial potential energies of the samples are indicated by the arrows. The data points show the evolution of the potential energy, $E_N^{t_a}$, as a function of cycle number N for samples for which $t_a = 10$ ps or 200 ps. The initial quench rates are: $Q_1 = 10^9 \text{ K s}^{-1}$, $Q_2 = 10^{10} \text{ K s}^{-1}$, $Q_3 = 10^{11} \text{ K s}^{-1}$, $Q_4 = 10^{12} \text{ K s}^{-1}$, $Q_5 = 10^{13} \text{ K s}^{-1}$. The other TC parameters are: $T_a = 400 \text{ K}$ ($= 0.54 T_g$, where $T_g \approx 740 \text{ K}$), $t_b = 100 \text{ ps}$, $T_b = 1 \text{ K}$, Q_a and $Q_b = 2.5 \times 10^{14} \text{ K s}^{-1}$.

Fig. 2 The steady-state potential energy E_s of $\text{Cu}_{50}\text{Zr}_{50}$ glasses reached when they are subjected to TC. The curve of E_s as a function of t_a is independent of the initial (as-quenched) state, and it intersects the values (dashed lines) of the initial potential energy of glasses formed by quenching at the indicated rates Q_i . The downward arrows show the crossover times t_c . When $t_a < t_c$ the as-quenched sample is rejuvenated through TC, and when $t_a > t_c$ it is relaxed.

Fig. 3 Effects of ageing and rejuvenation on atomic structures and mechanical properties. A $\text{Cu}_{50}\text{Zr}_{50}$ glass formed by quenching at 10^{13} K s^{-1} is treated by TC with $t_a = 10$ ps and 200 ps to attain steady-state potential energies respectively lower than (aged) and higher than (rejuvenated) the initial as-quenched glass (Supplementary Fig. 2). **(a)** The distributions of local shear and bulk modulus for each glassy state. **(b)** The difference radial distribution functions and (in the inset) the radial distribution functions for the same three glasses. **(c)** The relative populations of the most favoured Voronoi clusters. **(d)** The strain-stress curves for deformation in simple shear at 10^7 s^{-1} .

Fig. 4 Vibrational behaviour in glasses subjected to TC. **(a)** The vibrational density of states $g(E)/E^2$ after 0, 5, 20 and 50 cycles, showing evolution (arrowed) of the boson peak. The change in potential energy ΔE (inset) increases until a steady state is achieved; the data points for 5, 20 and 50 cycles are highlighted in blue, red and green, respectively. **(b)** The Pearson correlation coefficient $p_{0,N}$ of the atomic participation ratio P_i for the as-quenched state and after N cycles decays with N . The Pearson correlation coefficient $p_{N-1,N}$ of P_i for two adjacent cycled states (inset) also decays

with N . Three-dimensional spatial distributions of P_i in the as-quenched state **(c)**, and after one cycle **(d)**; regions with notable differences between the two states are circled.

Fig. 5 The influence of hold time t_b at low temperature. **(a)** The probability distribution of local temperature $T_{b,loc}$ at low temperature $T_b = 1$ K for $t_b = 20$ ps, 200 ps, ∞ (quasi-equilibrium). **(b–d)** The corresponding 3D spatial distributions of $T_{b,loc}$ at the end of the low-temperature hold.

Fig. 6 The progress of rejuvenation in one thermal cycle. **(a)** The evolution of potential energy in one cycle between high and low temperature, i.e. cooling from T_a down to T_b , holding at T_b , then heating back to T_a . The evolution is shown for two values of cooling/heating rate: 10^{10} K s⁻¹ (black line) and 10^{14} K s⁻¹ (red line). **(b)** The relation between the change in potential energy $\Delta E_P (= E - E_0)$ and the change in kinetic energy ΔE_K during the heating stage. The solid line is followed for Cu₅₀Zr₅₀ glass and crystal CuZr at $Q_a = 10^{14}$ K s⁻¹ applying the Nosé-Hoover (NH) thermostat; the dashed line is followed for the MG at $Q_a = 10^{10}$ K s⁻¹ applying the NH thermostat, and at $Q_a = 10^{14}$ K s⁻¹ applying the Langevin thermostat. **(c)** The change in energy as a function of the number of cycles for the three cases in (b) with $Q_a = 10^{14}$ K s⁻¹.

Fig. 7 The local activated rate (R_i). **(a)** The temperature evolution during the heating stage in one thermal cycle for the MG applying the Nosé-Hoover (NH) or Langevin (L) thermostats, and for CuZr crystal applying the NH thermostat. The circled region indicates the point at which the distributions of R_i are calculated. Contour plots of the 3D spatial distributions of R_i : **(b)** for crystal CuZr, applying the NH thermostat; **(c)** for the MG, applying the L thermostat; and **(d)** for the MG, applying the NH thermostat. The simulation is controlled by the NVT ensemble and $Q_a = 2.5 \times 10^{14}$ K s⁻¹.

Fig. 8. Local activated rate (R_i) and local non-affinity (\bar{D}_i). **(a)** Distributions of R_i for the MG and crystal CuZr applying the Nosé-Hoover (NH) thermostat, and for the MG applying the Langevin thermostat. The distributions are sampled at the reference point (circled) in Fig. 7a, over a time interval of 1 ps. **(b)** The correlation between \bar{D}_i and R_i for the three cases in (a): NH MG (red), Langevin MG (orange), and NH crystal (green), with Pearson correlation coefficients of 0.6, 0.06, and -0.03 respectively.

Fig. 9 Evolution of the local non-affinity (\bar{D}_i) during the hold at T_a . Contour plots of the 3D spatial

distributions of local non-affinity between the start of the hold (circled region in Fig. 7a) and after hold times Δt of **(a)** 0.2 ps, **(b)** 1 ps, **(c)** 4 ps, and **(d)** 80 ps.

Figure 1

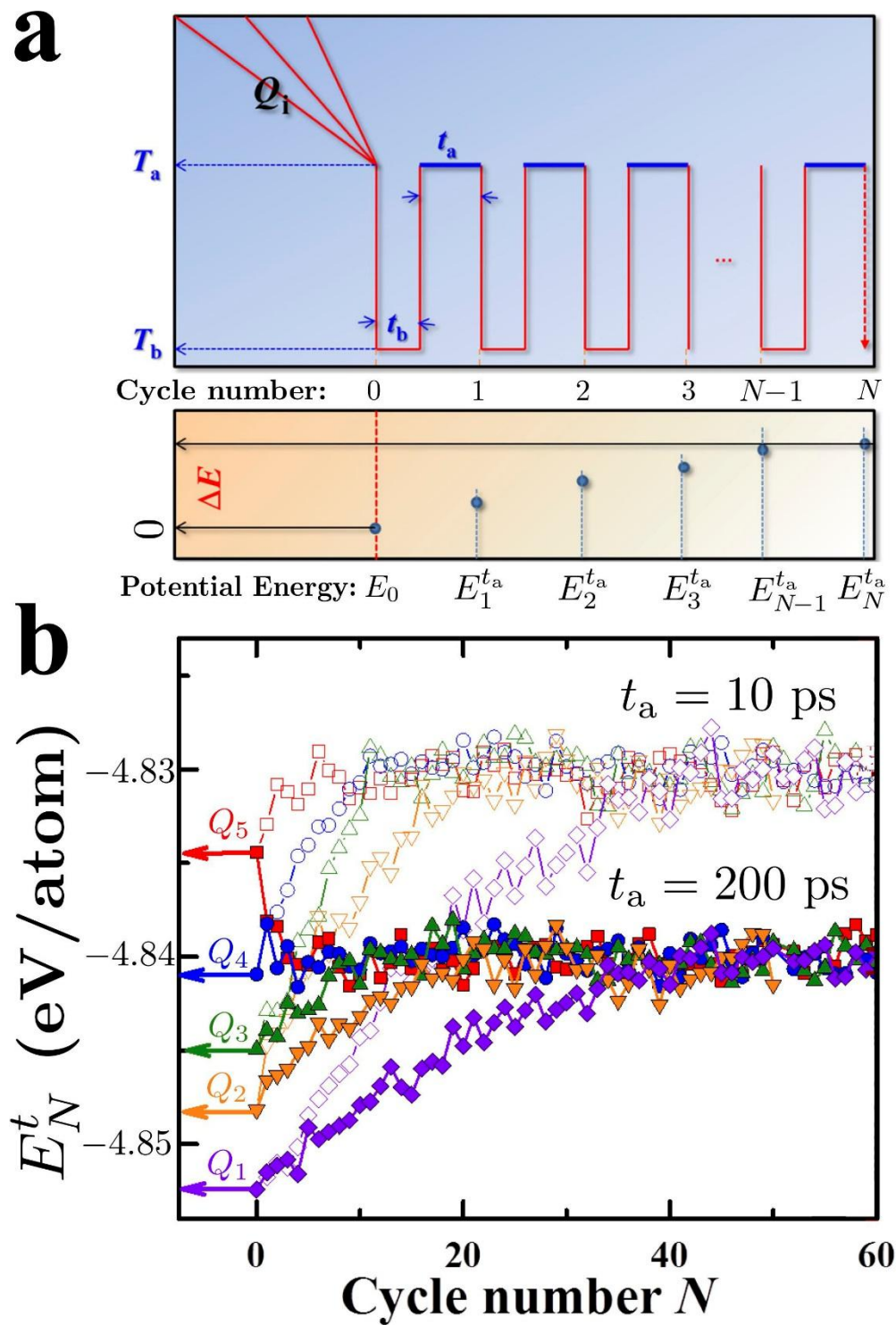


Figure 1. Shang et al

Figure 2

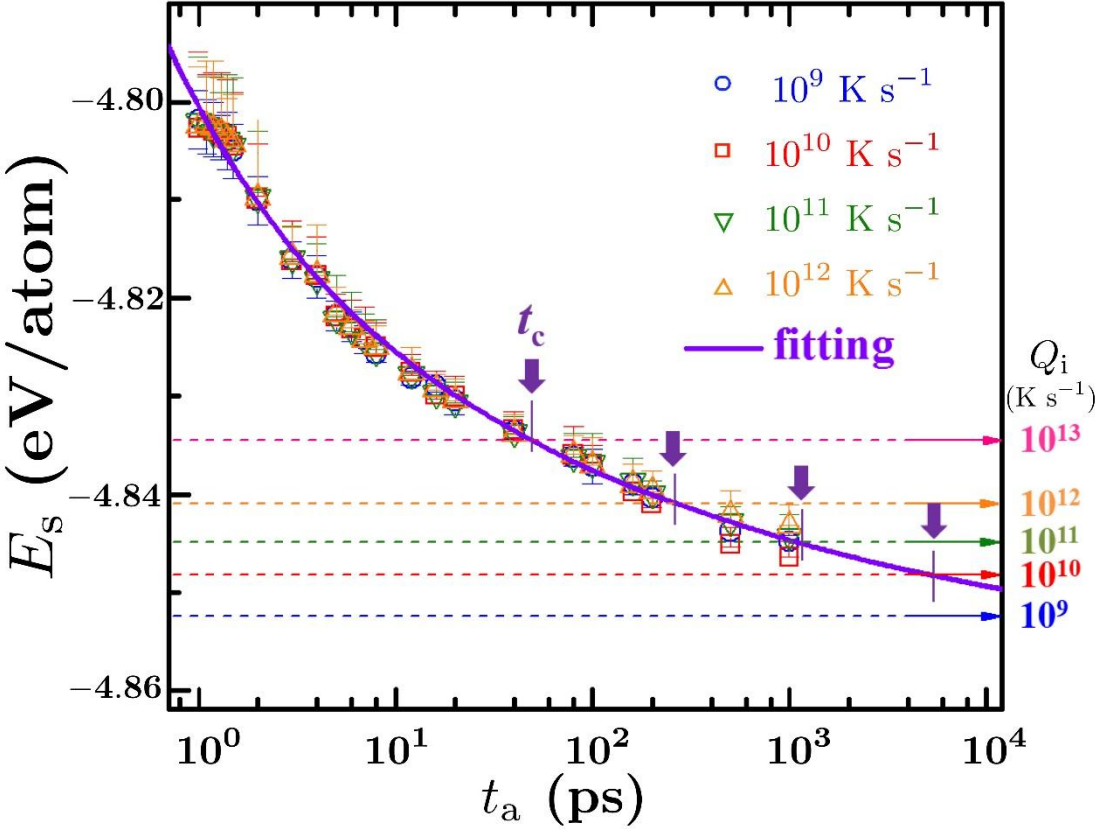


Figure 2. Shang et al

Figure 3

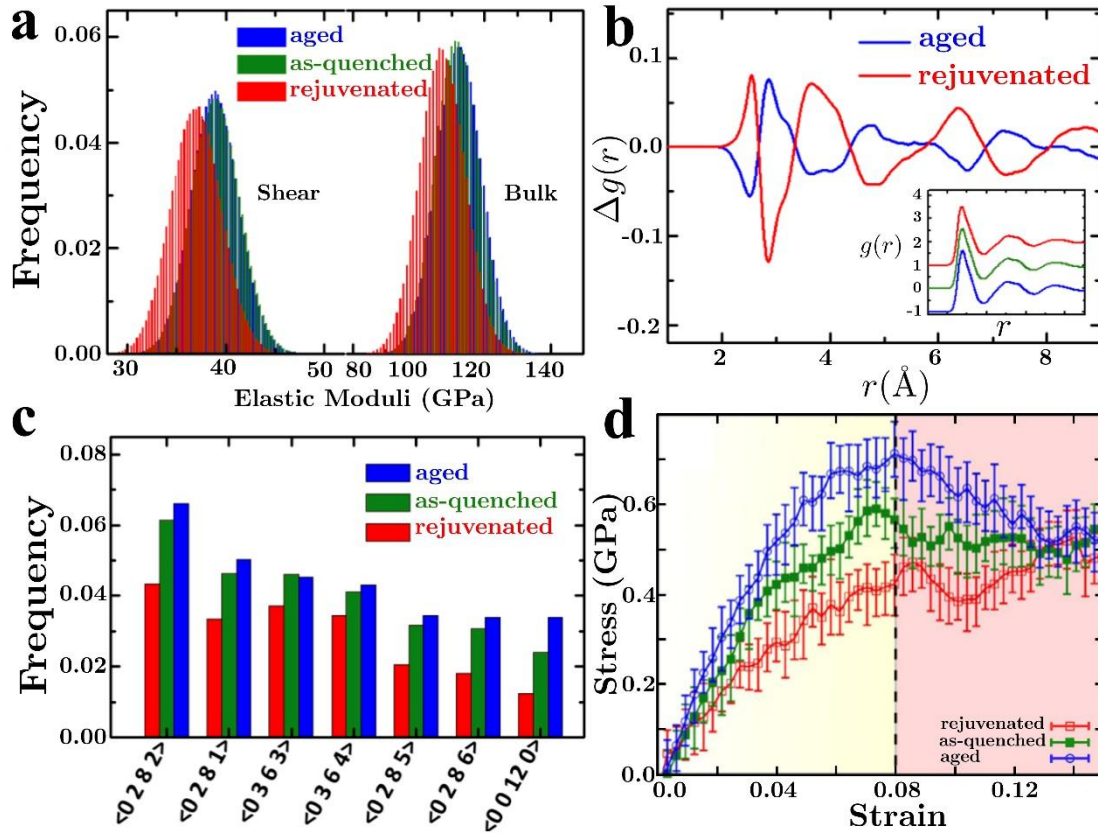


Fig. 3 Shang et al

Figure 4

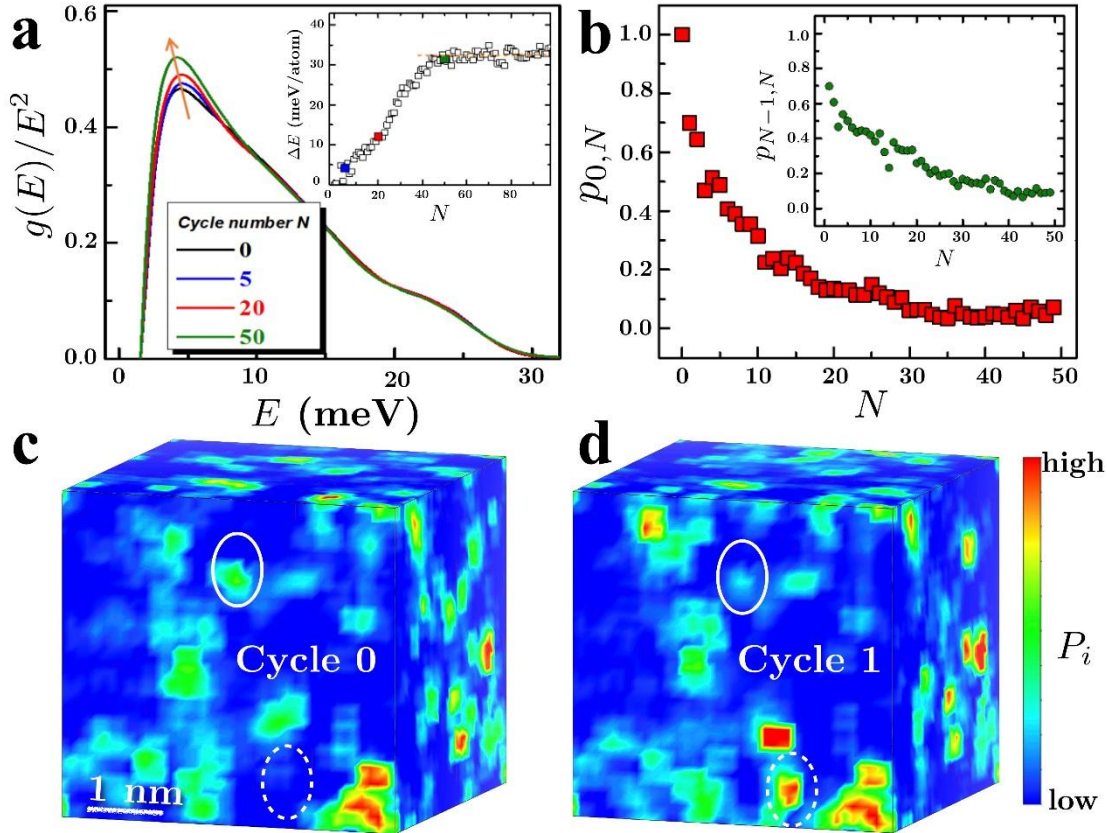


Fig. 4 Shang et al

Figure 5

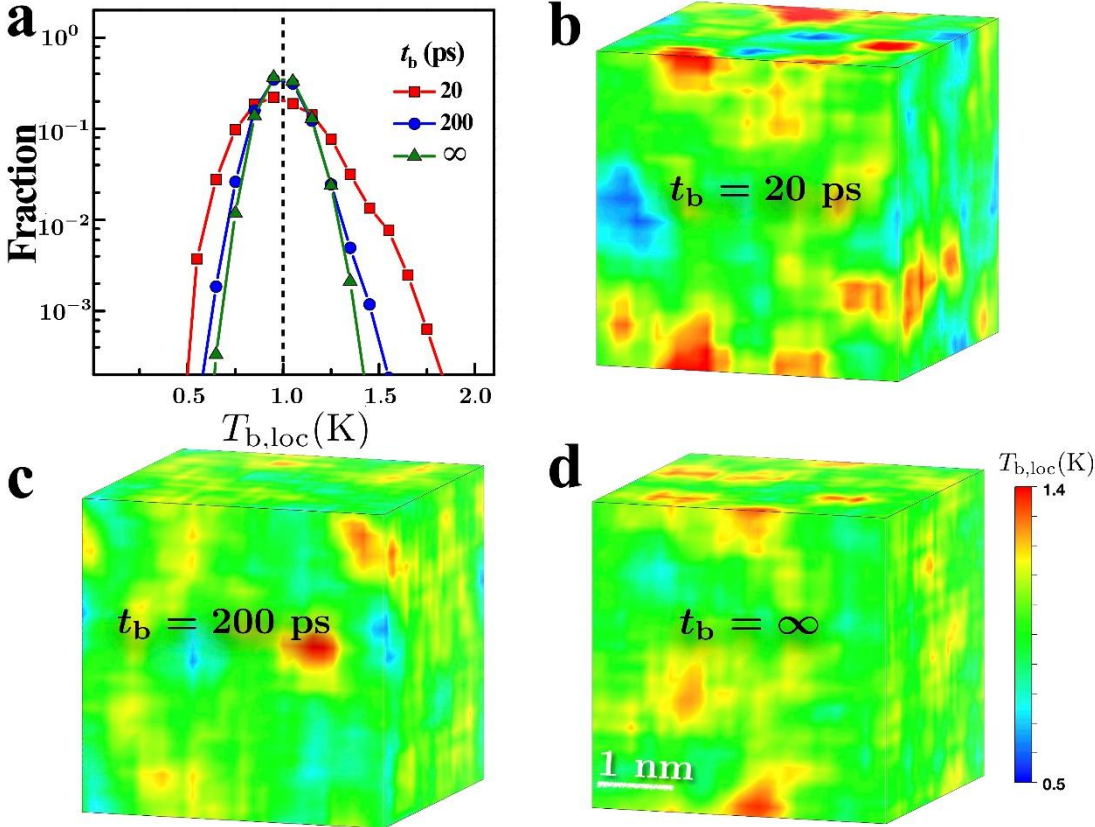


Fig. 5 Shang et al

Figure 6

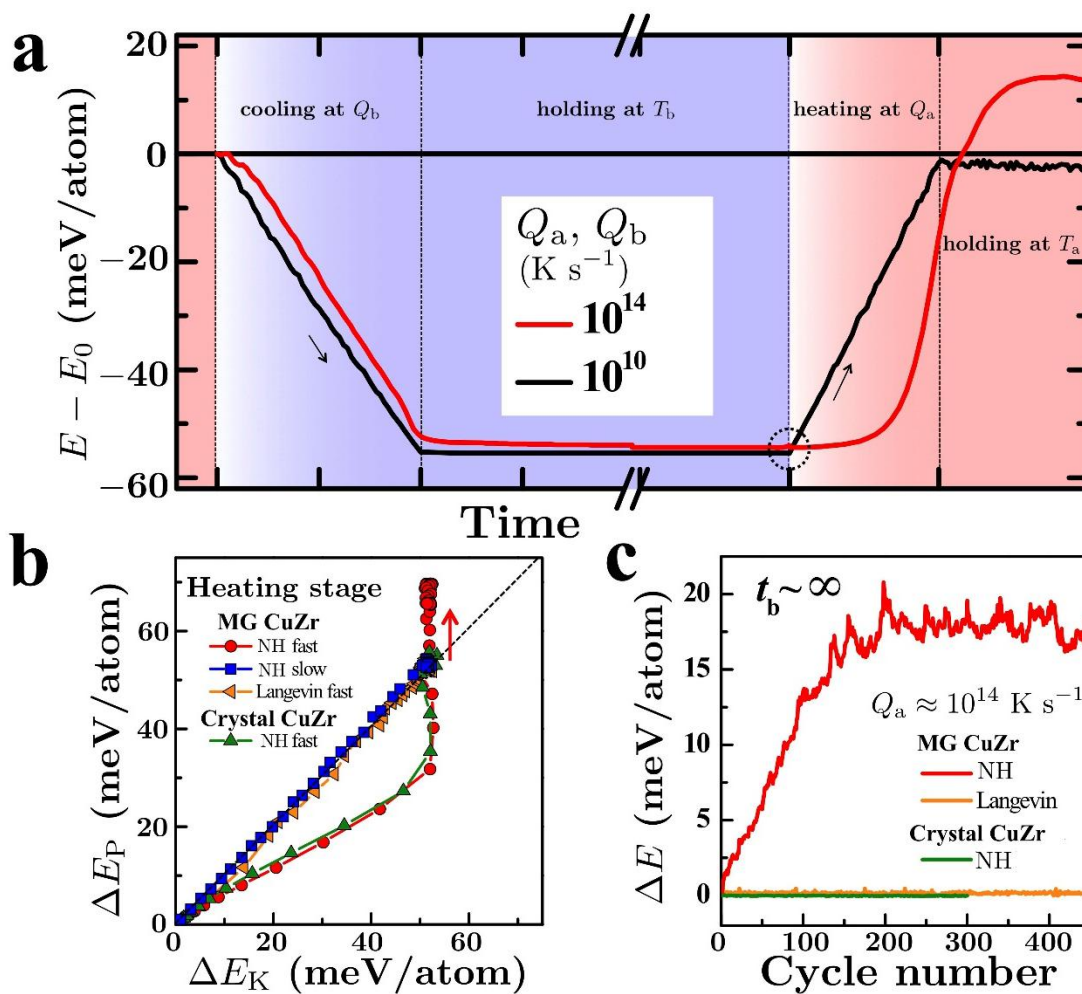


Fig. 6 Shang et al

Figure 7

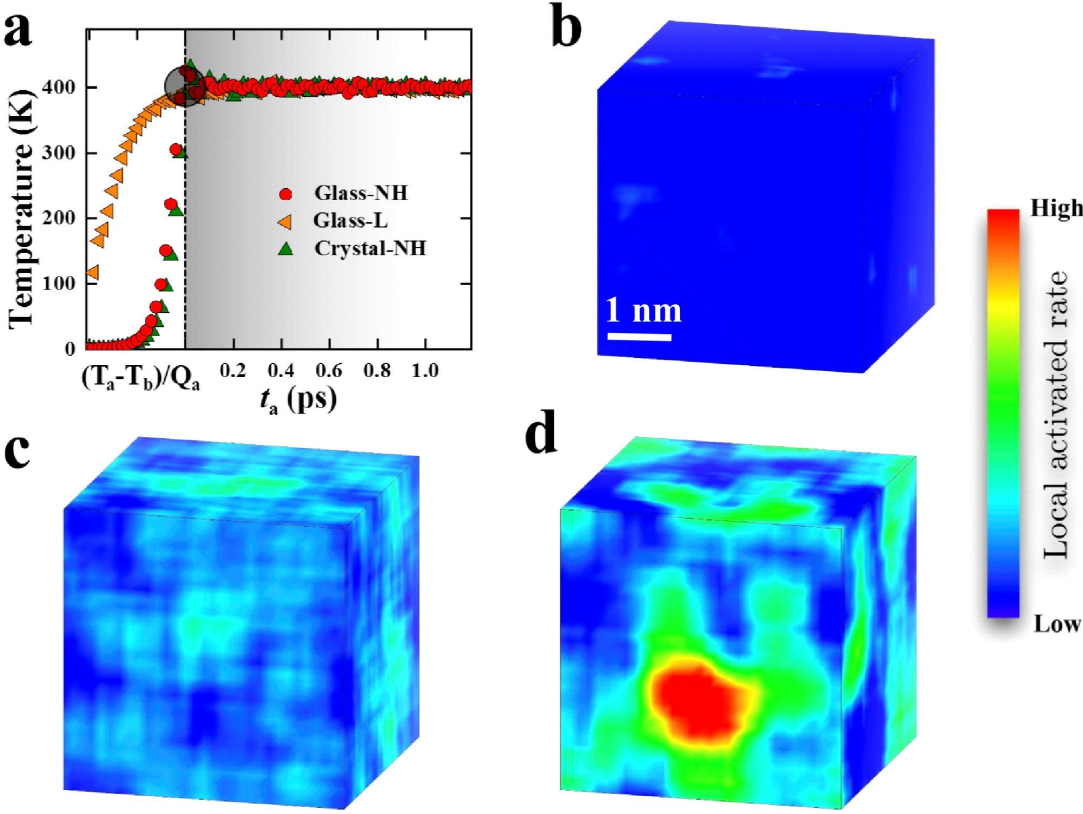


Fig. 7 Shang et al

Figure 8

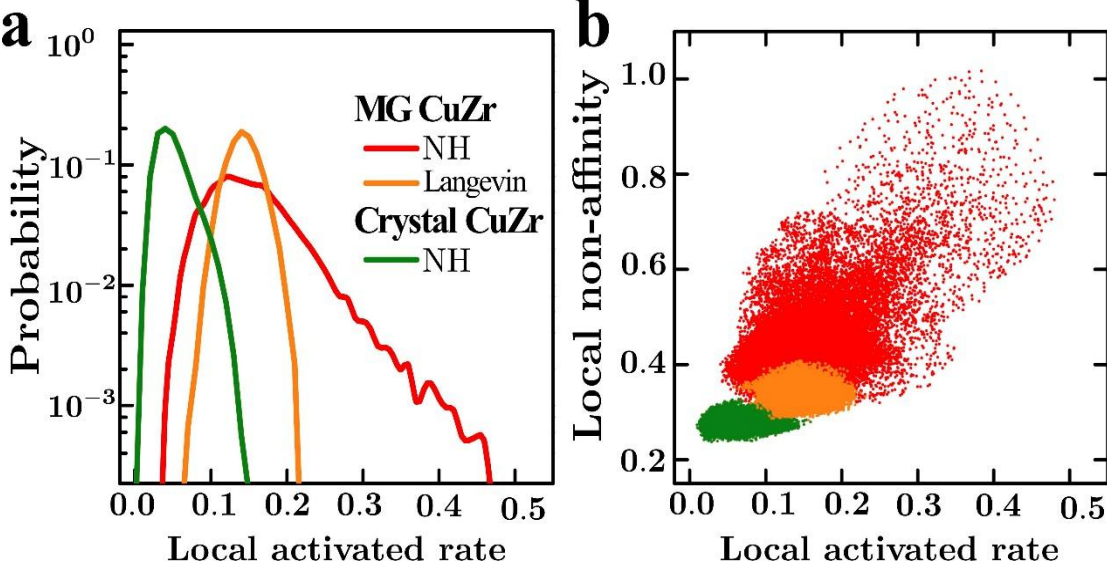


Fig.8 Shang et al

Figure 9

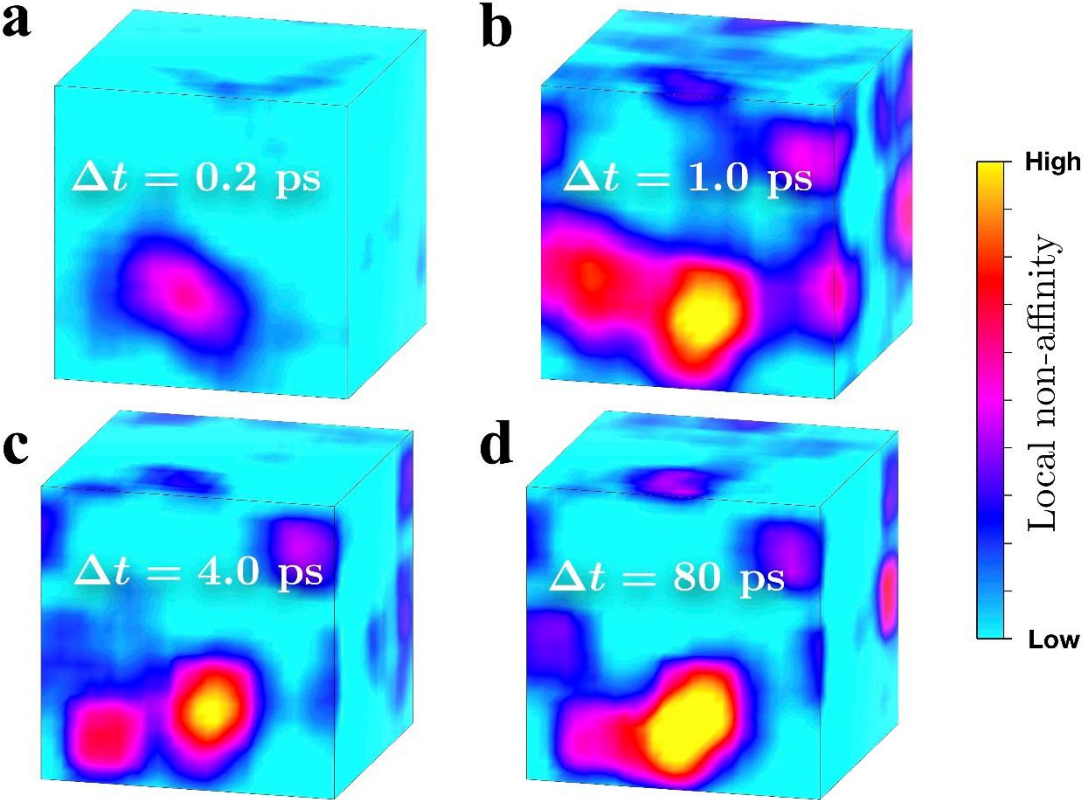


Fig.9 Shang et al

SUPPLEMENTARY MATERIALS:

Atomistic Modelling of Thermal-Cycling Rejuvenation in Metallic Glasses

Baoshuang Shang,^{1,2} Weihua Wang,^{3,2} Alan Lindsay Greer,⁴ and Pengfei Guan^{1*}

¹ *Beijing Computational Science Research Center, Beijing 100193, China*

² *Songshan Lake Materials Laboratory, Dongguan 523808, China*

³ *Institute of Physics, Chinese Academy of Sciences, Beijing 100190, China*

⁴ *Department of Materials Science and Metallurgy, University of Cambridge,*

27 Charles Babbage Road, Cambridge CB3 0FS, UK.

*pguan@csrc.ac.cn

1. Ageing versus rejuvenation during thermal cycling

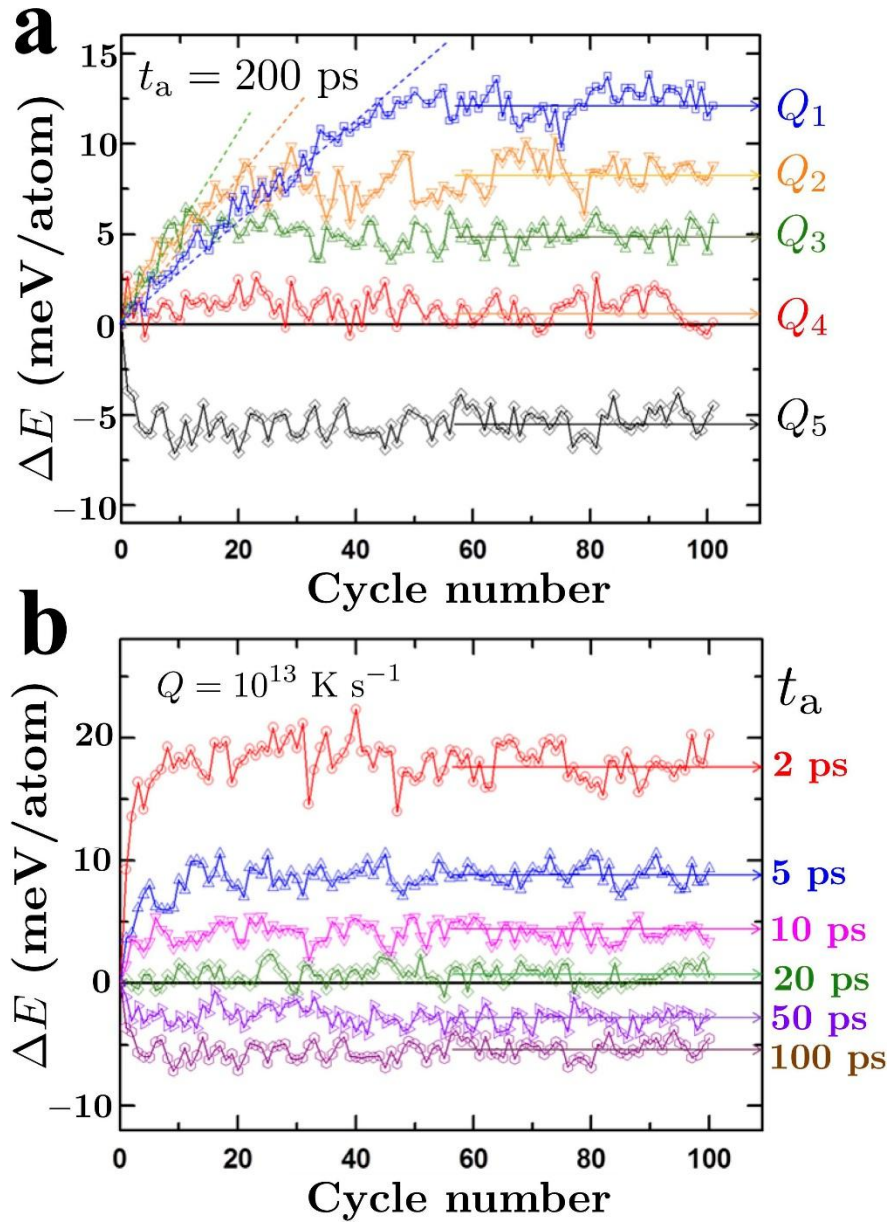


Fig. S1 The change in potential energy of $\text{Cu}_{50}\text{Zr}_{50}$ MG as a function of TC. **(a)** The change in energy ΔE as a function of the number of cycles N with $t_a = 200$ ps for samples prepared by quenching at different rates from $Q_1 = 10^9 \text{ K s}^{-1}$ to $Q_5 = 10^{13} \text{ K s}^{-1}$. **(b)** ΔE as a function of N for samples prepared at Q_5 and held for different times t_a at the upper temperature. Reheating/cooling rate $Q_a = Q_b = 2.5 \times 10^{14} \text{ K s}^{-1}$, $T_b = 1 \text{ K}$, $t_b = 200$ ps and $T_a = 400 \text{ K}$.

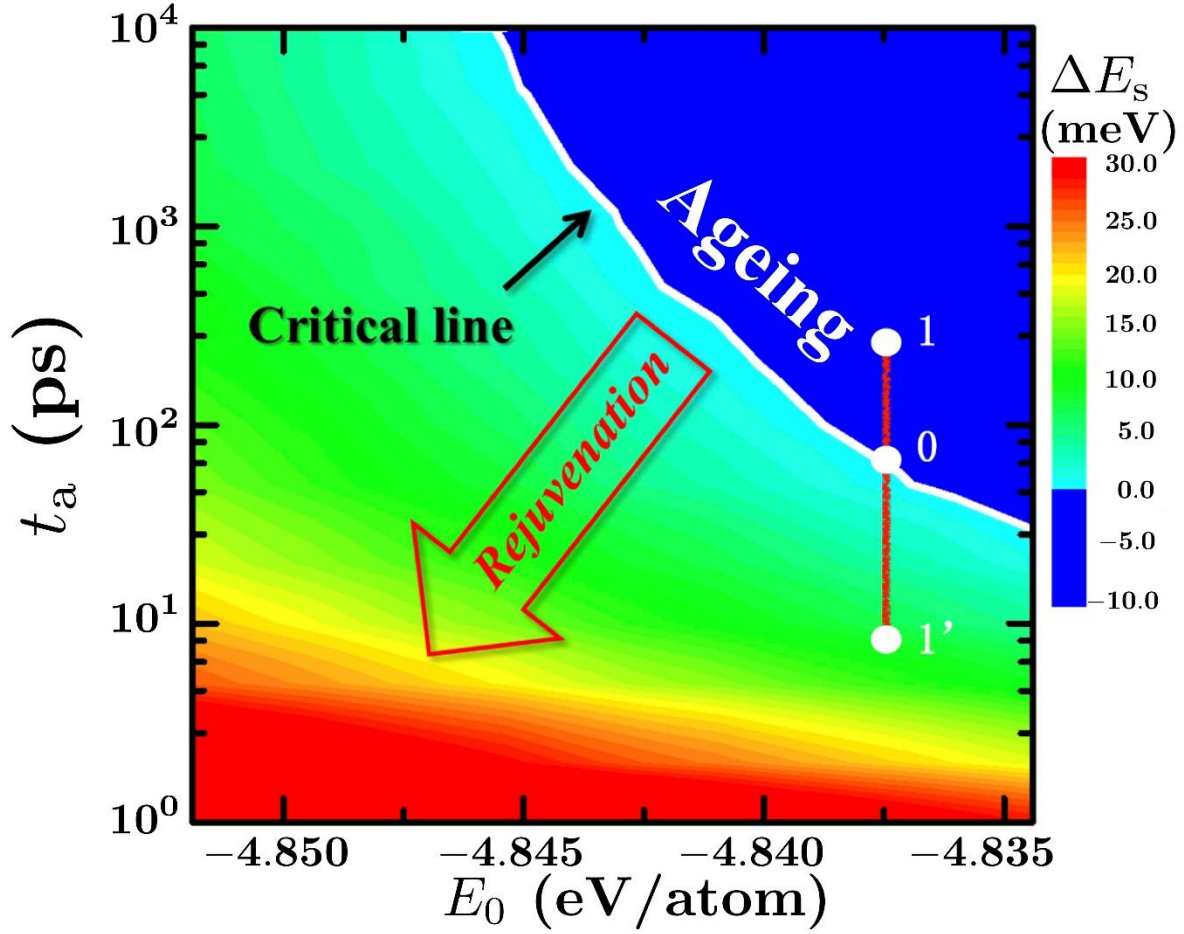


Fig. S2 Map of the potential energy change ΔE induced by TC. The value of ΔE depends on the energy E_0 of the initial as-quenched glass and on the hold time t_a at the upper temperature. The three points on the map represent: (1) a relaxed (aged) sample for which ΔE is negative, (0) the as-quenched sample, and (1') a rejuvenated sample for which ΔE is positive. Reheating/cooling rate $Q_a = Q_b = 2.5 \times 10^{14} \text{ K s}^{-1}$, $T_b = 1 \text{ K}$, $t_b = 200 \text{ ps}$ and $T_a = 400 \text{ K}$.

2. VDOS of thermally cycled samples

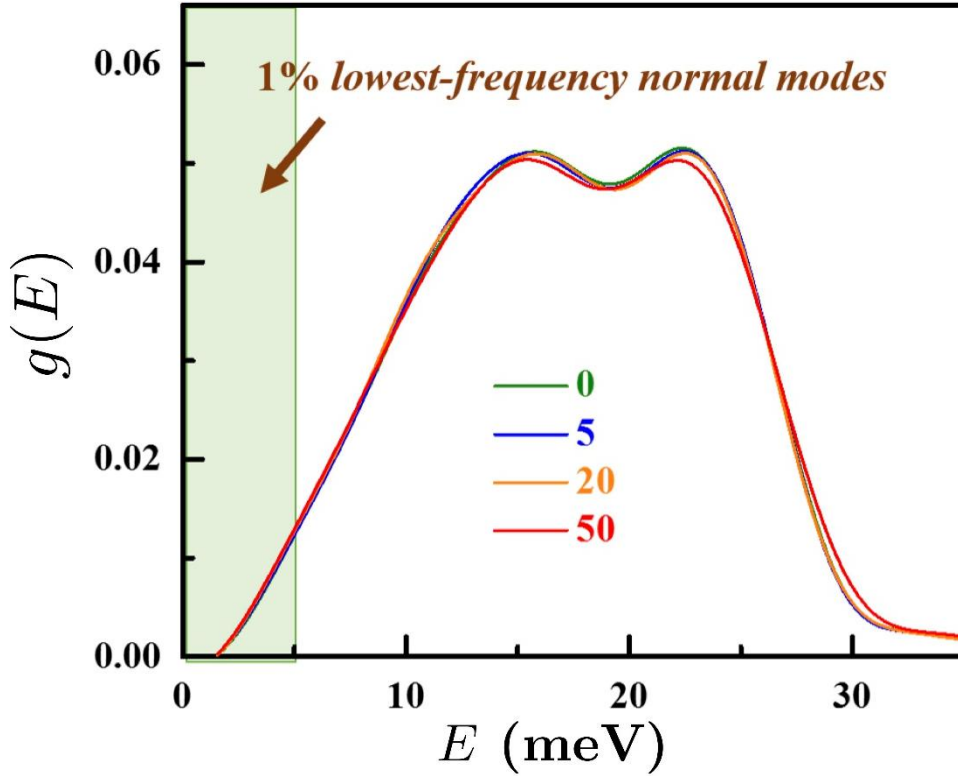


Fig. S3 The distribution of the vibrational density of states (VDOS) for an as-quenched sample and samples after 5, 20 and 50 thermal cycles. The shaded area shows the fraction of the distribution used to calculate the atomic participation ratio P_i . The default values are: reheating/cooling rate $Q_a = Q_b = 2.5 \times 10^{14} \text{ K s}^{-1}$, $t_b = 200 \text{ ps}$, $t_a = 4 \text{ ps}$, $T_b = 1 \text{ K}$ and $T_a = 400 \text{ K}$.

3. The evolution of soft spots in TC

In TC, the soft spots in metallic glasses can be activated, and during the atomic rearrangement they can be produced or annihilated. There are examples of both disappearance and generation of soft spots (dashed circles in Fig. S4), but overall an increase in their population. With increasing number of cycles the increased population reaches saturation. For the initial few cycles (Fig. S4), most soft spots are still stable, indicating that the rejuvenation is quite localized. In contrast, when the population density of soft spots reaches saturation, the spatial distribution is noticeably shuffled; this is caused by a sequence of interactions between soft spots.

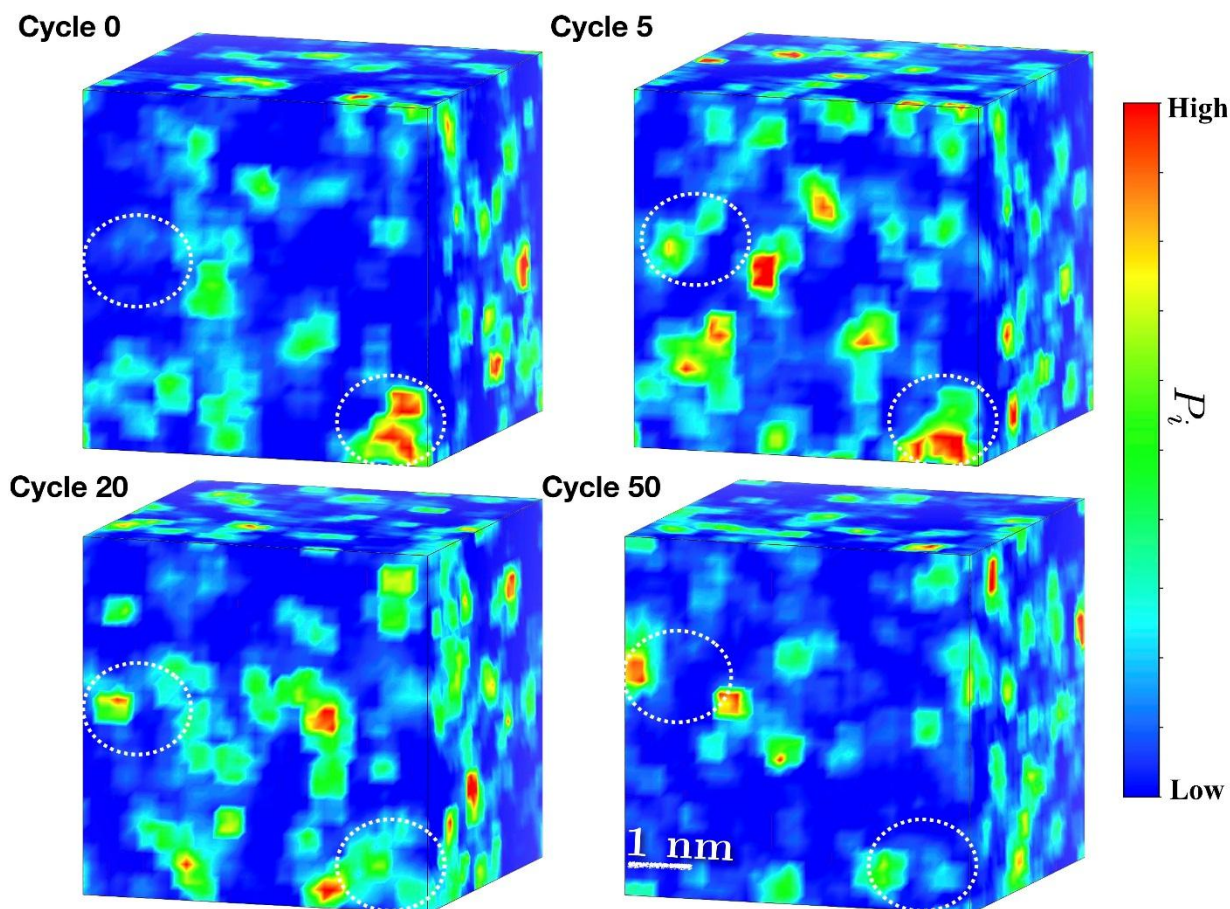


Fig. S4 Evolution of the distribution of the atomic participation ratio (P_i) upon TC. Contour plots of the 3D spatial distributions of P_i : (a) in the as-quenched state, and in states after (b) five, (c) 20, and (d) 50 cycles. The initial glass is formed by quenching at $Q_1 = 10^9 \text{ K s}^{-1}$. The default values are: reheating/cooling rate $Q_a = Q_b = 2.5 \times 10^{14} \text{ K s}^{-1}$, $t_b = 200 \text{ ps}$, $t_a = 4 \text{ ps}$, $T_b = 1 \text{ K}$ and $T_a = 400 \text{ K}$.

4. The definition of key parameters in TC

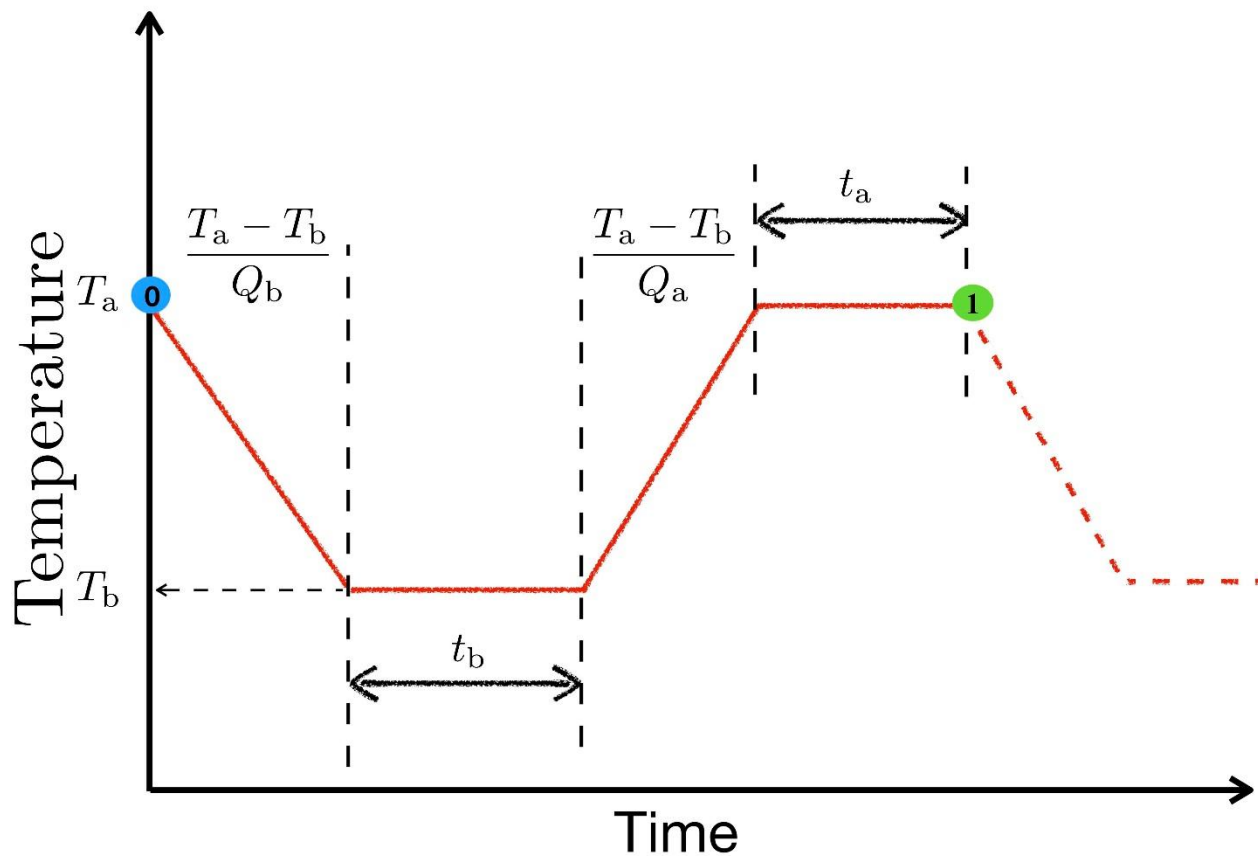


Fig. S5 The parameters in thermal cycling (TC). Each cycle starts from the blue point (state 0) and is characterized by the cooling rate Q_b , the hold time t_b at the lower temperature T_b , the heating rate Q_a , and the hold time t_a at the upper temperature T_a , and ends at the green point (state 1).

5. The influence of key factors on the rejuvenation

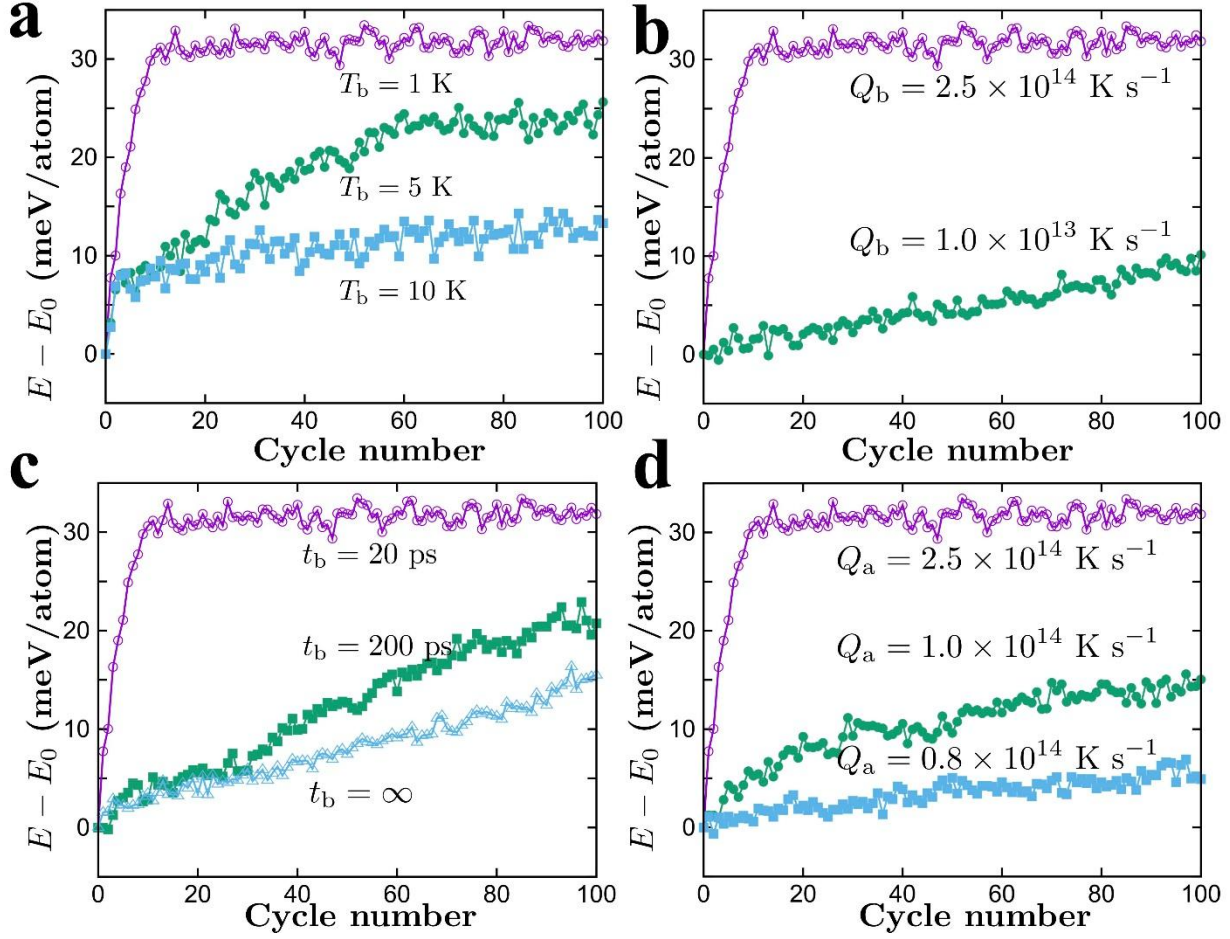


Fig. S6 Factors influencing the extent of rejuvenation induced by TC. Key factors are: **(a)** the lower temperature T_b , **(b)** the cooling rate Q_b , **(c)** the hold time t_b at the lower temperature, and **(d)** the heating rate Q_a .

6. The influence of the thermostat

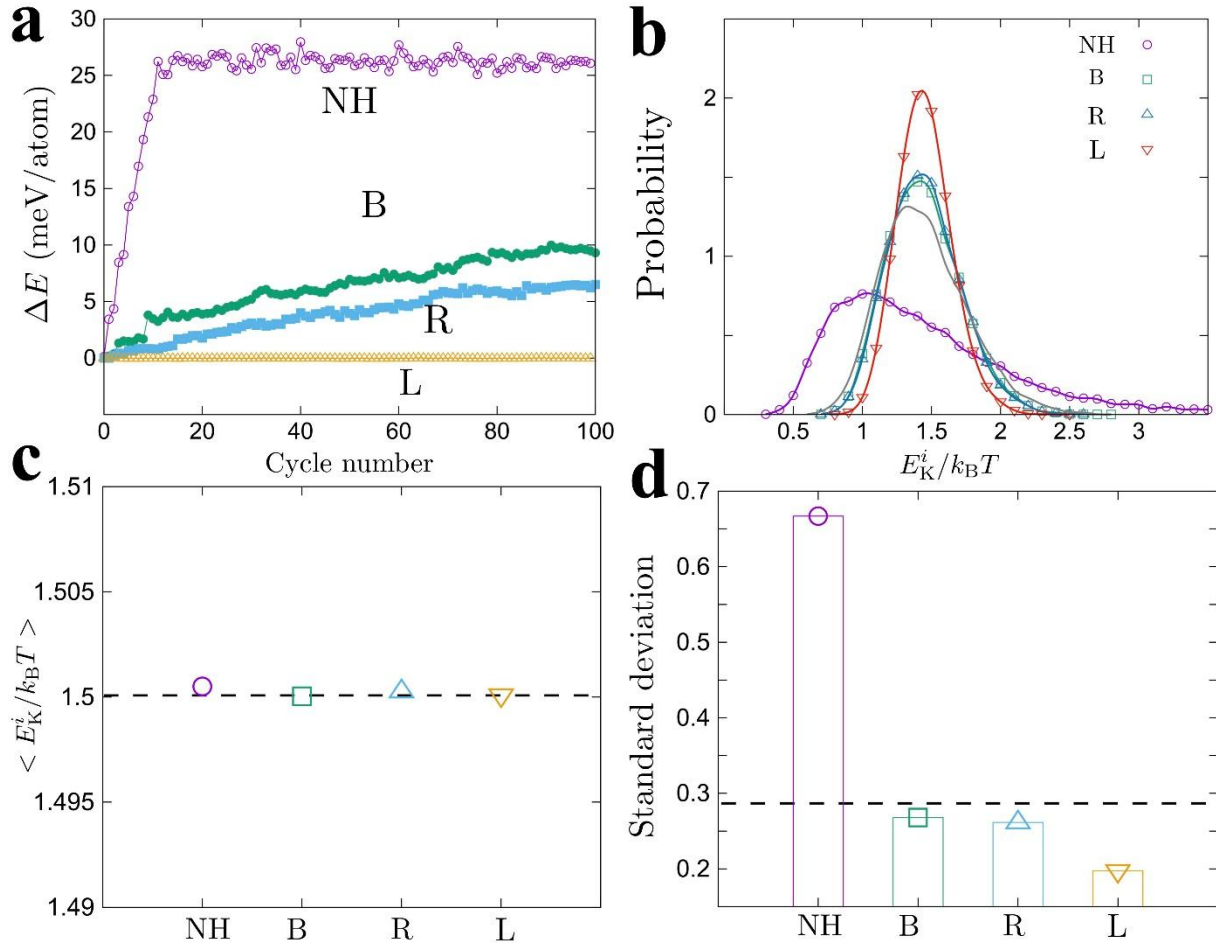


Fig. S7 The influence of the thermostat in simulations of thermal cycling of MG. **(a)** Evolution of potential energy at 1 K with cycle number for Nosé-Hoover (NH), Berendsen (B), rescaled (R) and Langevin (L) thermostats. **(b)** The distributions of local kinetic energy $E_K^i/k_B T$ at the start of the first heating stage under different thermostats; the initial state (atomic configuration and atomic kinetic energy distribution) at the start of the first hold t_b is the same for all thermostats. **(c)** The average of the local kinetic energy $\langle E_K^i/k_B T \rangle$ for different thermostats. The dashed line shows the value of $\langle E_K^i/k_B T \rangle$ in the initial state, which suggests that E_K^i fluctuates around 1 K for all thermostats. **(d)** The standard deviation of the distribution of the local kinetic energy $E_K^i/k_B T$. The dashed line presents the standard deviation of the initial state, the spatial distributions of E_K^i are shown in Fig. 5b. The default values are: reheating/cooling rate $Q_a = Q_b = 2.5 \times 10^{14} \text{ K s}^{-1}$, $t_b = 200 \text{ ps}$, $t_a = 4 \text{ ps}$, $T_a = 400 \text{ K}$ and $T_b = 1 \text{ K}$.

As shown in Fig. S7a, the degree of rejuvenation is highly dependent on the choice of thermostat. In MD simulations, the thermostat is intended to mimic the processes of ‘equilibration’ in the physical world. It is difficult to say which of various possible thermostats best represents the physical world in a highly non-equilibrium heating process. However, the basic principle should be consistency between MD and the physical world with regard to different degrees of rejuvenation.

When the distribution of local kinetic energy at the start of the *first heating stage* is more heterogeneous (Fig. S7b, d), the degree of rejuvenation during heating is greater. For the Nosé-Hoover thermostat, the heterogeneity is greatly enlarged after heating while, in contrast, the Berendsen and the rescaled thermostats maintain the initial heterogeneity. Since the Langevin thermostat controls the temperature by a stochastic equation, the heterogeneity of local kinetic energy is maintained at the lowest level, and there is no correlation with the initial state. The mean value of the local temperature is identical in all cases. Thus, there is a special role for the heterogeneity of local kinetic energy, which, in addition to the glassy structure itself, can also drive the rejuvenation or relaxation.

7. The effect of bulk thermal expansion in simulations

Due to the heterogeneous structure of metallic glasses, non-uniform thermal expansion has been considered as the origin of rejuvenation in cryogenic thermal cycling (CTC). In our MD simulations and previous work [11], we find that the probability of activation by the local thermal expansion mismatch is quite small. If we suppress bulk thermal expansion during TC by fixing the sample volume, the efficiency of rejuvenation does not change significantly (Fig. S8), that is to say, bulk thermal expansion is unnecessary for CT induced rejuvenation. There is a role for structural heterogeneity, but not for overall volume change.

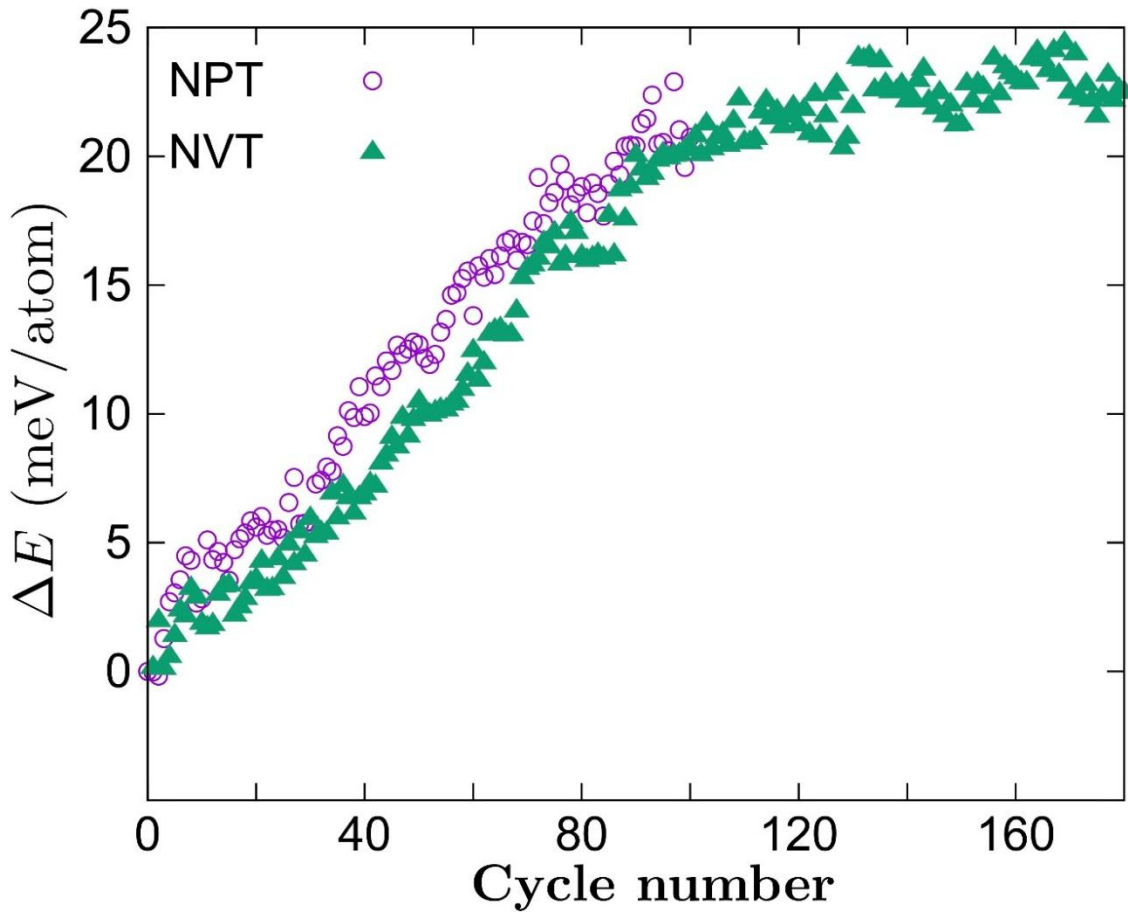


Fig. S8 Comparison of the NVT and NPT ensembles in simulations of the effects of TC. The increase in potential energy ΔE is similar in each case. The temperature is controlled by the Nosé-Hoover thermostat, the pressure is controlled by the Parrinello-Rahman barostat, $T_a = 400$ K, $T_b = 1$ K, $Q_a = Q_b = 2.5 \times 10^{14}$ K s⁻¹, $t_b = 200$ ps and $t_a = 4$ ps.